



Activation of Nrf2 in fibroblasts promotes a skin aging phenotype via an Nrf2-miRNA-collagen axis



Paul Hiebert^a, Anastasiya Martyts^b, Jonas Schwestermann^a, Katharina Janke^c,
Jürg Hafner^d, Petra Boukamp^c, Edoardo Mazza^b and Sabine Werner^a

a - Department of Biology, Institute of Molecular Health Sciences, ETH Zurich, Zurich 8093, Switzerland

b - Department of Mechanical and Process Engineering, Institute for Mechanical Systems, ETH Zurich, Zurich 8092, Switzerland

c - Department of Environmentally-Induced Skin and Lung Aging, IUF - Leibniz Research Institute for Environmental Medicine, Düsseldorf 40225, Germany

d - Department of Dermatology, University Hospital Zurich, Zurich 8091, Switzerland

Corresponding author. paul.hiebert@biol.ethz.ch.

<https://doi.org/10.1016/j.matbio.2022.09.002>

Abstract

Aging is associated with progressive skin fragility and a tendency to tear, which can lead to severe clinical complications. The transcription factor NRF2 is a key regulator of the cellular antioxidant response, and pharmacological NRF2 activation is a promising strategy for the prevention of age-related diseases. Using a combination of molecular and cellular biology, histology, imaging and biomechanical studies we show, however, that constitutive genetic activation of Nrf2 in fibroblasts of mice suppresses collagen and elastin expression, resulting in reduced skin strength as seen in aged mice. Mechanistically, the “aging matrisome” results in part from direct Nrf2-mediated overexpression of a network of microRNAs that target mRNAs of major skin collagens and other matrix components. Bioinformatics and functional studies revealed high NRF2 activity in aged human fibroblasts in 3D skin equivalents and human skin biopsies, highlighting the translational relevance of the functional mouse data. Together, these results identify activated NRF2 as a promoter of age-related molecular and biomechanical skin features.

© 2022 The Author(s). Published by Elsevier B.V. This is an open access article under the CC BY license (<http://creativecommons.org/licenses/by/4.0/>)

Introduction

Nuclear factor erythroid 2-related factor 2 (NRF2) is a transcription factor best known for its crucial role in mediating the cellular antioxidant response through activation of various cytoprotective target genes [1–4]. During homeostasis, NRF2 activity is inhibited by binding to the KEAP1 protein, which facilitates its proteasomal degradation in the cytoplasm. When cells become challenged or stressed, the accumulation of electrophiles and/or reactive oxygen species (ROS) disrupts the KEAP1-NRF2 interaction, allowing newly synthesized NRF2 to enter the nucleus and facilitate the transcription of its target genes by binding to antioxidant-response elements (AREs) in their promoter/enhancer regions [3,5]. The NRF2 pathway has therefore generated

intense interest as a potential therapeutic target whose activation may help to prevent diseases where ROS play a pathological role [6].

Oxidative stress is generally thought to increase with age and to contribute to multiple age-related diseases [7,8]. In the skin, aging is typically associated with reduced synthesis and enhanced degradation of dermal ECM. This particularly affects the main ECM components of the skin, such as the collagens type I and III and elastin, resulting in weakening of the dermis and overall skin fragility [7,9]. Current dogma suggests that NRF2 activity declines with age, which may contribute to the corresponding increase in persistent oxidative stress in many tissues [10]. Therefore, pharmacological activation of NRF2 is considered as a potential anti-aging strategy [11]. However, the uniformity with which NRF2

activity changes with age in different tissues or cell types is unclear, and the consequences of NRF2 activation for skin aging are unknown.

Research on the role of NRF2 in aging and disease often involves the use of NRF2 activating compounds. These can provide useful insights and also have therapeutic potential, but their impact on multiple signaling pathways often make the exact contribution of NRF2 difficult to determine. Furthermore, they lack the ability to distinguish the consequences of NRF2 activation in specific cell types. Previously, mice were generated, which allow expression of a constitutively active form of Nrf2 (caNrf2) in a cell type- and tissue-specific manner [12,13]. The caNrf2 mutant lacks the binding site for Keap1, but retains the other functional domains of the protein. This mutant has been extensively characterized, and activates Nrf2 to a similar level as in wild-type cells that are treated with Nrf2 activating compounds [13–15]. This has also been shown in fibroblasts, where caNrf2 expression or pharmacological activation of endogenous Nrf2 leads to suppression of cell proliferation and induction of cellular senescence due in part to Nrf2-mediated transcription of matrix genes, such as the gene encoding plasminogen activator inhibitor 1 [16]. However, the mechanisms behind the regulation of other ECM genes, particularly genes that are negatively regulated by Nrf2, including different collagens [16], are unknown. In addition, the consequences of these alterations for skin function remain to be determined.

Here, we identified over 100 significantly upregulated miRNAs in skin fibroblasts in response to constitutive Nrf2 activation, with top hits serving to regulate ECM structure and function by suppressing collagen and elastin expression. As a consequence, the mechanical properties of mouse skin were severely affected, with consequences similar to the skin fragility syndrome seen in aged human skin, which can become extremely severe in some individuals [17]. Our data suggest that while Nrf2-mediated collagen suppression may have benefits for scarring and fibrosis [16], the altered matrix may also aggravate weakening of the skin and susceptibility to skin tearing, which are commonly associated with advanced age.

Results

Constitutive activation of Nrf2 in fibroblasts inhibits collagen deposition in mouse skin

To investigate the impact of constitutive Nrf2 activation on the production and organization of ECM in the skin, we made use of mice expressing caNrf2 in fibroblasts in a Cre-dependent manner (see

experimental procedures) [16]. The expression levels of classical Nrf2 target genes in cultured fibroblasts of these mice and the resulting functional alterations are comparable to those of wild-type cells that are treated with Nrf2-activating compounds [16]. Therefore, these mice are an ideal model to study the consequences of Nrf2 activation.

A proteomics analysis of the matrixome from cultured primary fibroblasts from caNrf2 mice had revealed a strong down-regulation of various collagens compared to control cells [16]. Since collagen is the most abundant ECM protein, we examined the impact of caNrf2 on collagen production *in vivo* using skin from 10-week-old mice. Total collagen content was significantly reduced in the skin of caNrf2 mice, which correlated with a reduction in skin weight (Fig. 1A). There was also a small difference in collagen per wet weight (Fig. 1A). Next, we determined if and how reduced collagen levels in caNrf2 mice affect histological properties of the skin from shortly after birth to adulthood. Picosirius Red staining of skin sections from control mice at postnatal day 2.5 (P2.5) showed very little collagen relative to adult skin (Fig. S1A). A further reduction of total collagen fibers was observed in P2.5 caNrf2 mice in comparison to ColCre-wt (ctrl) mice (Fig. 1B). Reduced collagen type I deposition in newborn skin of caNrf2 mice was confirmed by immunofluorescence staining (Fig. S1B). Picosirius Red staining looked more similar in ctrl and caNrf2 mouse skin by the time mice reached adulthood (10 weeks), with caNrf2 mice showing only a small, but non-significant reduction in the amount of red/thick collagen fibers (Fig. 1B). When we examined the pattern of collagen fibers using Picosirius Red-stained skin sections in more detail [18,19], we again found differences between ctrl and caNrf2 mouse skin shortly after birth, particularly in curvature and high-density matrix parameters, as well as in the overall orientation of collagen fibers (Figs. S1C and 1C). However, these differences were no longer detected when mice reached adulthood (Fig. S1D,E).

For a more thorough investigation of collagen in the skin of adult caNrf2 and ctrl mice, we examined fresh, unfixed skin sections using multi-photon microscopy and second harmonic generation (SHG). Both forward and backward SHG signals were obtained (Fig. S1F). The ratio of forward (F-SHG) to backward (B-SHG) signals can be used to gain insight into the relative size and orientation of collagen fibrils [20,21]. It was significantly lower in the caNrf2 mouse skin (Fig. 1D), suggesting thinner fibrils compared to ctrl skin [20,21]. A lower F-SHG/B-SHG ratio may also indicate that collagen fibers in caNrf2 skin are oriented more in the lateral direction, as opposed to the more axially oriented fibers in the ctrl skin [20,21]. SHG images were also used to investigate the ECM pattern in adult mouse skin [18,19]. Unlike Picosirius Red-stained sections,

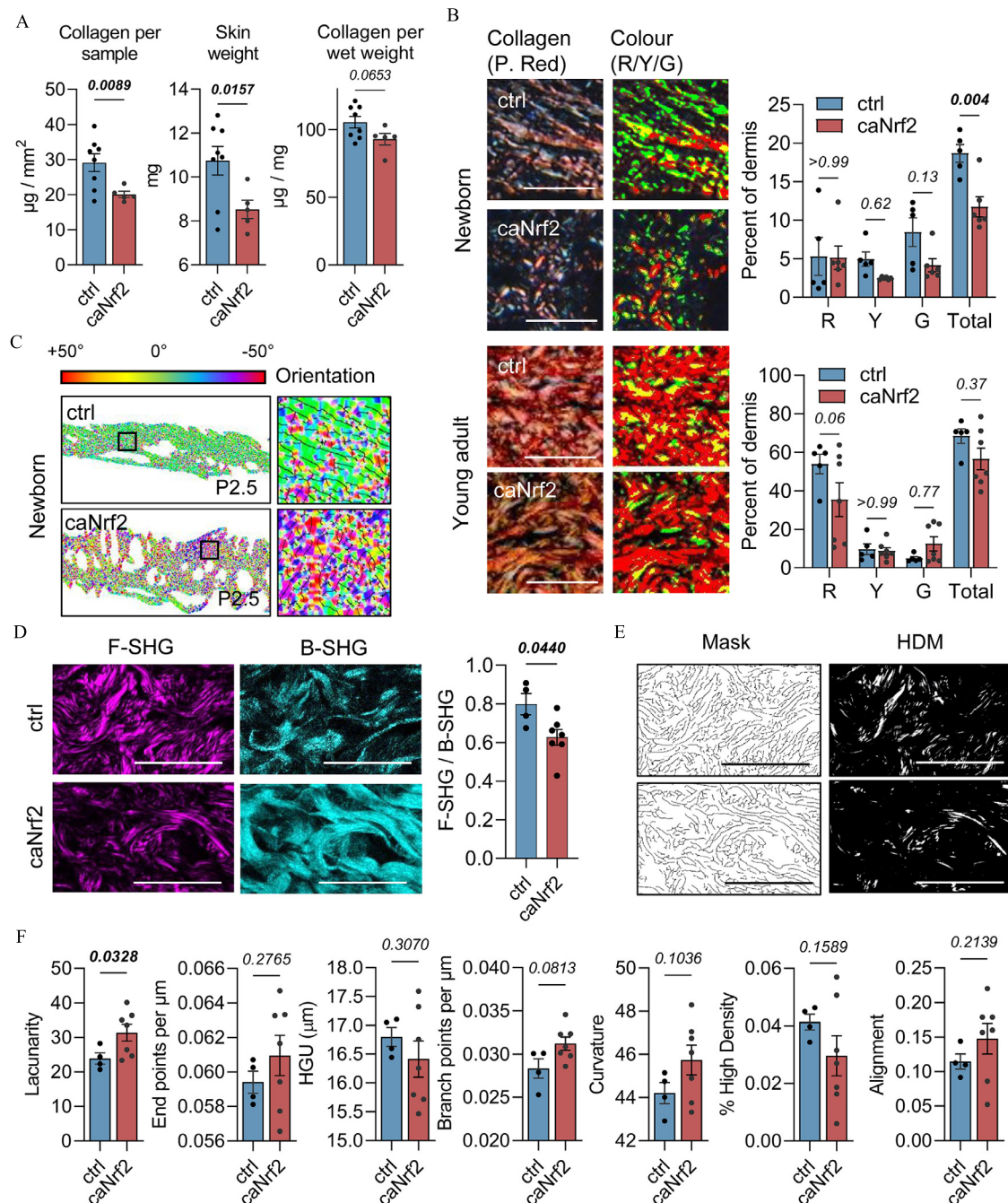


Fig. 1. Constitutive *Nrf2* activation in fibroblasts alters collagen deposition and arrangement. (A) Total collagen content, skin weight and collagen per wet weight measured from two 5 mm diameter back skin biopsies from 10-week-old male mice. $N = 5-8$ pairs of skin biopsies from different mice. (B) Picosirius Red staining of back skin from newborn (P2.5) and adult (10 weeks) mice and quantification of differently sized fibers based on their color: R=red, Y=yellow, G=green. $N = 5-7$ skin samples from different mice. (C) Images depicting the orientation of fibers set to color (newborn mice, P2.5). (D) Representative SHG images of skin sections from ctrl and caNrf2 mice taken in either the forward (F-SHG) or backward (B-SHG) direction. Intensities were used to calculate the F-SHG/B-SHG ratio. $N = 4-7$ skin samples from different mice. (E) Images corresponding to those in (D) of the generated mask used to calculate the measurements pertaining to ECM pattern, and the generated image used to quantify high density fibers. Images were obtained using the TWOMBLI plugin for ImageJ [18]. (F) Analysis of collagen structure and pattern based on images collected using F-SHG. $N = 4-7$ skin samples from different mice. Values were obtained using the TWOMBLI plugin for ImageJ [18]. Bar graphs show mean \pm s.e.m. Numbers above bars show exact p-values (Welch's t-test (A, D, F) and two-way ANOVA with Sidak's multiple comparisons test (B)). Significant differences are indicated in bold. Scale bars = 25 μm .

fresh/unfixed SHG images showed significantly more lacunarity in caNrf2 mouse skin (Fig. 1E and F).

Overall, these results suggest that caNrf2 mice have reduced collagen deposition, which is associated with an altered ECM content, organization and structure in newborn and also adult skin.

mRNA levels of major ECM proteins are reduced in fibroblasts with activated Nrf2

To see if the reduced ECM deposition in caNrf2 mouse skin results from alterations in the mRNA levels, we re-analysed RNA-seq data from cultured fibroblasts of these mice [16]. The most strongly expressed collagen genes in newborn mouse skin are *Col3a1*, *Col1a2* and *Col1a1*, followed by genes coding for collagen VI (*Col6a1*, *Col6a2* and *Col6a3*) and collagen V (*Col5a1*, *Col5a2*) (Fig. S2A) [22]. Expression of the vast majority of these genes was reduced in P2.5 caNrf2 mouse skin compared to ctrl mice, and similar observations were made in whole skin of adult mutant mice (Figs. 2A and S2B). The differences were even more pronounced when examining cultured primary fibroblasts isolated from newborn mouse skin (Figs. 2A and S2B). By contrast, analysis of matrix metalloproteinase (MMP) mRNA levels showed mixed results, with some slightly up-regulated, others down-regulated, and many showing no significant difference (Fig. S2C). Together, this suggests that the differences in Picrosirius Red staining observed in newborn mouse skin and the reduced collagen deposition by caNrf2 fibroblasts are likely a result of reduced collagen synthesis by these cells. A significantly reduced expression of the major skin collagens (*Col1a1*, *Col1a2*, *Col3a1*) was also observed when fibroblasts from wild-type mice were treated with different Nrf2-activating compounds for 24 h (Fig. 2B). This result further confirms the appropriate activity of the caNrf2 transgene and shows that regulation of collagen by activated Nrf2 occurs within a short period of time.

Fibroblasts with constitutively activated Nrf2 express an “aging matrisome”

Reduced collagen levels are a hallmark of aged skin [17,23,24]. Therefore, we determined if changes in mRNA levels that occur upon Nrf2 activation also occur in fibroblasts from wild-type mice upon aging. Gene set enrichment analysis (GSEA) of RNA sequencing (RNA-seq) data from caNrf2 fibroblasts [16] identified both up- and down-regulated genes as mildly enriched in published datasets of fibroblasts isolated from old mice (18 months of age) (Fig. 2C) [25]. Further analysis of genes making up the leading-edge subset revealed an enrichment for upregulated genes involved in cell

morphogenesis, platelet-derived growth factor receptor (PDGFR) signaling and chemotaxis (Fig. S3A). In contrast, downregulated “leading edge genes” encode proteins involved in collagen fibril organization and organization of the ECM in general, suggesting that changes in ECM represent one of the major age-related consequences of constitutive Nrf2 activation in skin fibroblasts (Fig. S3A). Examination of gene ontologies associated with upregulated genes in caNrf2 fibroblasts identified immune system processes and inflammatory response as the most frequently occurring terms (Fig. S3B). This is consistent with the chronic low-grade inflammation often documented in aged skin [26]. It also matches our previous observations that showed increased CD45⁺ immune cells in the skin of caNrf2 mice, and reduced CD45⁺ cells in mice with Nrf2-deficient fibroblasts [16]. Together, these results strongly suggest that Nrf2 activates a number of genes in fibroblasts that can affect age-related phenotypes.

To examine how caNrf2-induced changes in the production of ECM compare to that of fibroblasts from aged mouse skin, GSEA was performed using a filtered dataset from old skin fibroblasts of wild-type mice [25] that included only matrisome genes [27]. Both up- and downregulated genes in caNrf2 fibroblasts were strongly and significantly enriched, and to a much greater extent than when all genes were included (Fig. 2C). This suggests that constitutive Nrf2 activation mainly affects expression of ECM genes associated with aging.

Closer examination of leading-edge genes showed collagens and proteoglycans to be generally reduced, while upregulated genes were more often those encoding ECM regulators and other secreted factors (Fig. 2C). This was confirmed at the protein level by re-analyzing data generated from proteomic analysis of ECM deposited by caNrf2 fibroblasts [16], which showed the major skin collagens were reduced in the matrisome of caNrf2 fibroblasts (Fig. 2D), while MMP and TIMP levels in the deposited matrix were not or only mildly altered (Fig. S2D). The reduced expression of *Col1a1*, *Col1a2* and *Col1a3* in aged skin was confirmed by quantitative real-time PCR (qRT-PCR) using RNA isolated from the skin of old mice (20 months), which showed significantly reduced expression of these genes compared to young (10 weeks) controls (Fig. 2E).

Age-related changes in skin collagen mimic those seen in young caNrf2 mouse skin

To see how the ECM in aged skin of wild-type mice compares to caNrf2 mouse skin at the protein level, we performed a similar biochemical and imaging analysis of ECM/collagen content as was done on caNrf2 mouse skin. Similar to caNrf2 mouse skin, total collagen content was significantly lower in the

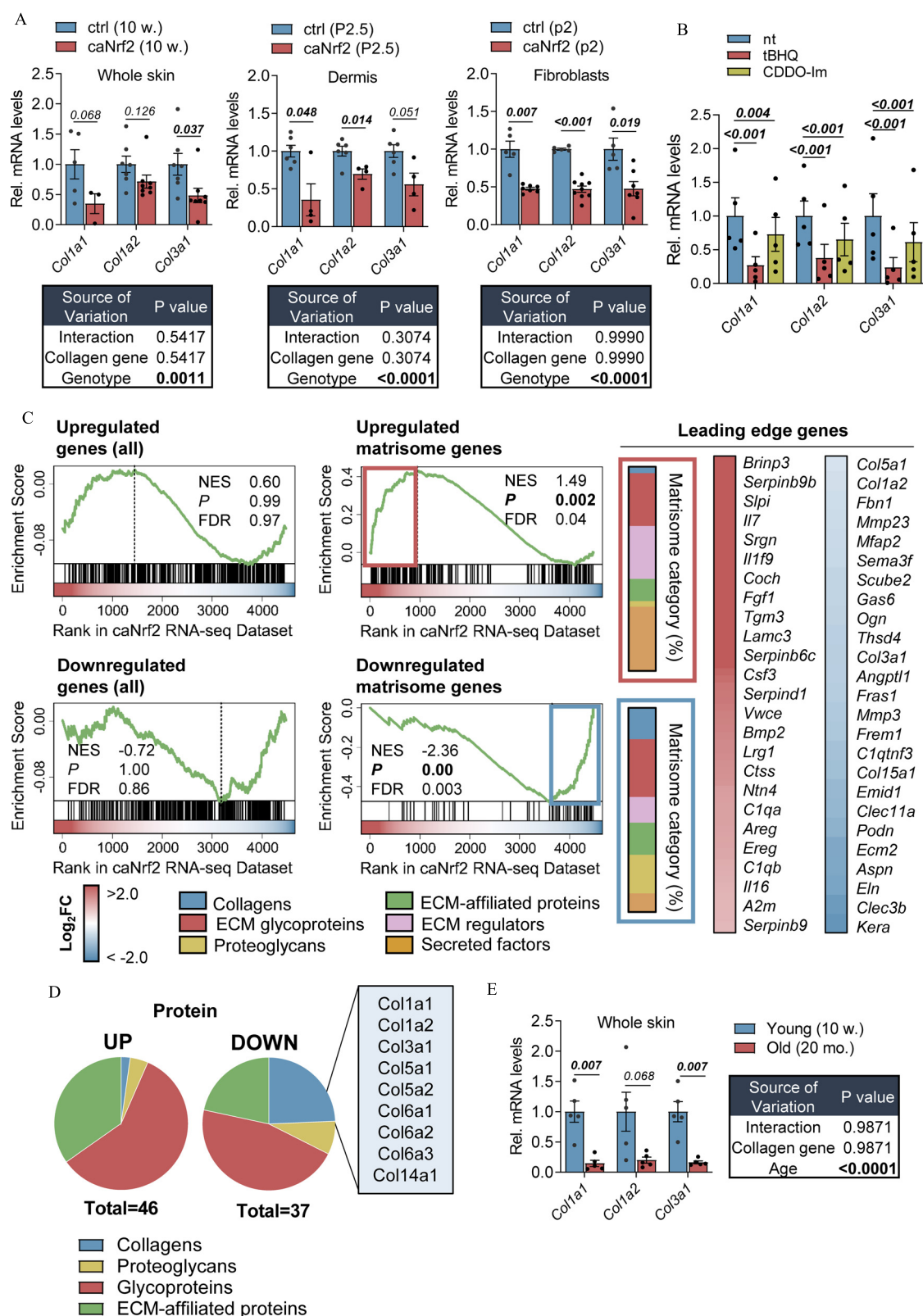


Fig. 2. caNrf2 fibroblasts express a matrisome with similarities to aged skin. (A,B) qRT-PCR for different collagens using RNA from whole skin of adult mice (ctrl vs. caNrf2), newborn mouse dermis (ctrl vs. caNrf2), primary skin fibroblasts (ctrl vs. caNrf2) and wild-type primary fibroblasts treated with the Nrf2 activating compounds tBHQ (50 μ M) or CDDO-Im (5 nM) for 24 h. $N = 4-8$ skin samples or cell cultures from different mice. (B) Genes regulated in caNrf2 vs. ctrl fibroblasts

skin of old (20 months) compared to young (10 weeks) wild-type mice, and also corresponded to reduced skin weight and a reduction in collagen per wet weight (Fig. 3A). However, no difference was observed in the thickness of the dermis between aged and young mouse skin (Fig. S4A). This is similar to what we have shown previously for 10-week-old *caNrf2* mice, which show similar skin thickness compared to ctrl mice of the same age [16]. Analysis of Picrosirius Red-stained skin sections also revealed similar dermal matrix patterns in old and young mice (Fig. S4B). When aged skin was examined using SHG, we observed a similar decrease in the F-SHG/B-SHG ratio as seen in young *caNrf2* mice, which may also point toward more laterally oriented fibers and thinner fibrils in aged skin (Figs. 3B and S4C) [20,21]. Like *caNrf2* mice, detailed analysis of the ECM pattern showed a significant increase in collagen lacunarity (Figs. 3C and S4D). In summary, age-related changes in skin collagen of aged wild-type mice strongly mimic those seen in the skin of young *caNrf2* mice.

Prolonged *Nrf2* activation reduces skin strength and stiffness reminiscent of aged skin

Collagens make up the majority of ECM protein in the skin, and collagen organization at different length scales largely determines the mechanical properties of the tissue [28–30]. Therefore, we investigated the functional consequences of age-related changes in skin collagen by examining the biomechanical properties of skin from old vs. young wild-type mice and from young *caNrf2* vs. ctrl mice. Strips of freshly excised murine back skin were stretched along the head-tail axis in a saline bath while measuring the applied force (Fig. 3D). Skin was first stretched to a predefined physiological force level and then held for 10 min to measure its relaxation (Fig. 3D, Movie S1). With the same force level applied, skin from old mice stretched to a similar distance as skin from young adult mice, and tension after 10 min of relaxation was similar (Fig. 3E). The results were similar when comparing 10-week-old *caNrf2* mice to ctrl mice of the same age (Figs. 3E and S4E). To examine the response of the skin to changes in osmolarity, the saline bath was

changed from an isotonic saline to a hyper- or hypotonic solution 2 min after the start of relaxation, and the specimens further relaxed in the respective solution until the end of the relaxation experiment. Skin from old mice responded to changes in osmolarity to a lesser extent compared to skin from young mice; however, this difference did not reach statistical significance (Fig. 3F and G). The difference was more pronounced in skin from *caNrf2* vs. ctrl mice, and the change in relative tension in response to a hyper- or hypotonic bath was significantly different to the control group (Figs. 3F,G and S4F, Movie S2). This suggests a lower fixed charge density in the skin of old wild-type mice and young *caNrf2* mice, possibly due to the amount and composition of glycosaminoglycans, and/or proteoglycans [31–33]. Indeed, several proteoglycans were down-regulated at the RNA and protein levels in *caNrf2* fibroblasts (Fig. 2C,D).

After relaxation, the skin samples were unloaded, then loaded again to the point of rupture, to characterize the whole tension-stretch curve up to rupture (Movie S3). Both *caNrf2* skin and skin from old mice failed with significantly less force than their respective controls (Figs. 3H and S4G). This is despite the fact that the stretch at rupture was similar in all cases (Figs. 3I and S4H), indicating a similar skin distensibility. The tension-stretch curves during loading to rupture show that young adult mice - both wild-type mice and the ctrl mice of the *caNrf2* colony - have the typical “J” shape, due to stiffening associated with progressive collagen fiber recruitment and elongation. By contrast, old wild-type mice and young *caNrf2* mice showed a flatter curve (Figs. 3J and S4I). In summary, the changes of the biomechanical properties of young skin in response to constitutive *Nrf2* activation in fibroblasts display characteristics that are strikingly similar to those that occur during aging in wild-type mice.

Nrf2 regulates microRNA expression in skin fibroblasts

While there are a few examples of *Nrf2* acting as a repressor of transcription [34], *Nrf2* primarily activates gene expression [3]. Therefore, we hypothesized that *Nrf2* induces the expression of

subjected to GSEA against gene sets from skin fibroblasts of old (18 months) vs. young (2 months) mice [25]. Analyses are included for all differentially regulated genes and specifically for matrisome genes. Normalized enrichment score (NES) is shown along with *p* value (*P*) and FDR *q*-value (FDR). The distribution of the different matrisome categories within each leading-edge subset, as well as the top 25 leading edge genes, are shown for both GSEA performed using matrisome genes. (C) Distribution of different categories of matrisome proteins that are differentially abundant in the matrisome of cultured *caNrf2* vs. ctrl fibroblasts (both up and down). (D) qRT-PCR for different collagens using RNA samples from the skin of young (10 weeks) vs. old (20 months) mice. *N* = 5 samples from different mice. Bar graphs show mean ± s.e.m. Numbers above bars show exact *p*-values (Welch's *t*-test (A,E), Two-way ANOVA with Sidak's multiple comparisons test (B)). Significant differences are indicated in bold.

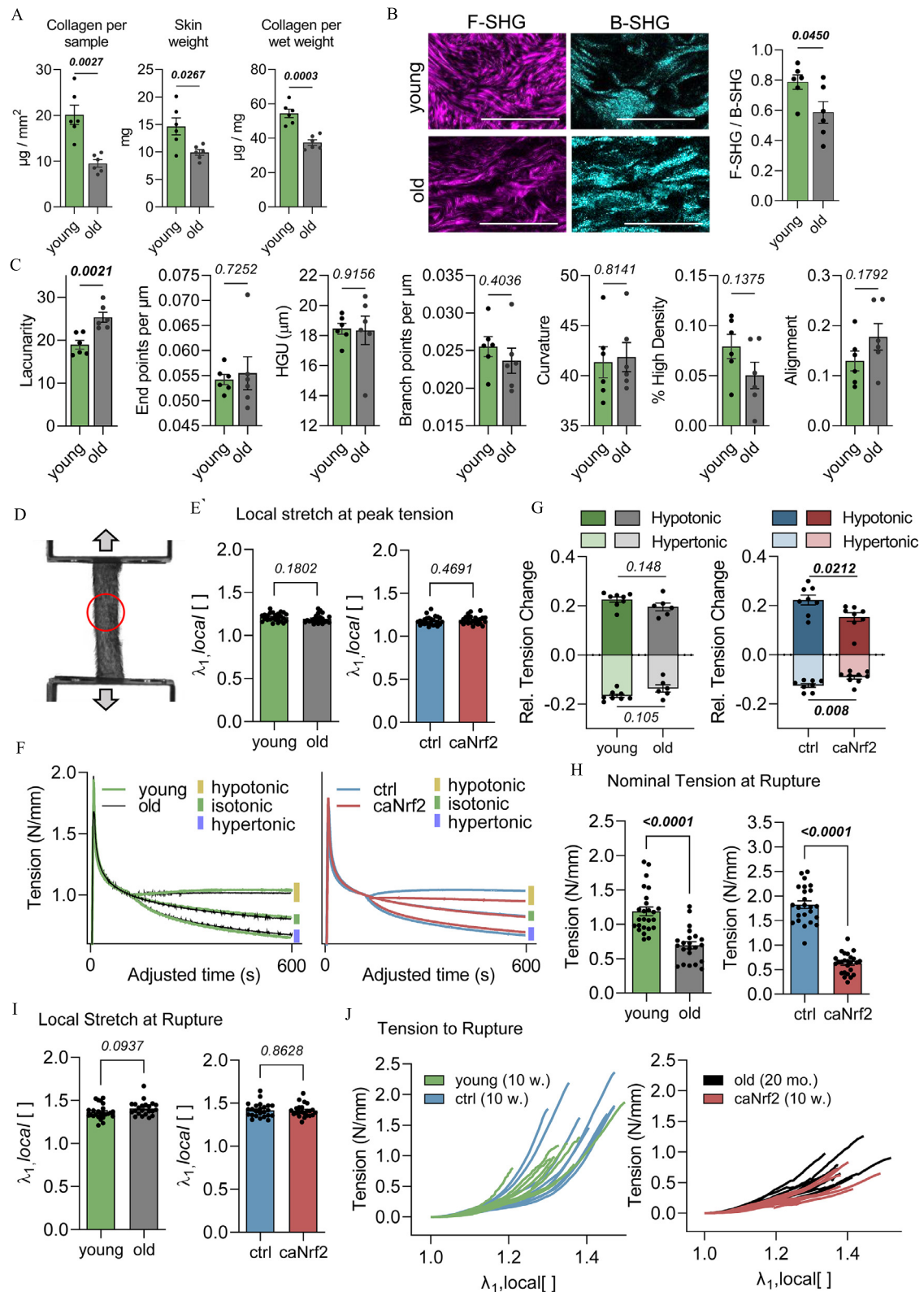


Fig. 3. Skin biochemical and biomechanical properties of caNrf2 mice mimic those of aged mice. (A) Total collagen content and weights measured from two 5 mm diameter back skin biopsies from young (10 weeks) or old (20 months) male mice. $N = 6$ pairs of skin biopsies each taken from different mice. (B) Representative SHG images of skin sections from young and old mice taken in either the forward (F-SHG) or backward (B-SHG) direction. Intensities were used to

microRNAs (miRNAs, miRs), which may target collagens. miR-sequencing (miR-seq) identified 117 significantly upregulated and 103 significantly downregulated miRs in early passage caNrf2 fibroblasts compared to controls (Figs. 4A and S5A, Table S1). Interestingly, the most strongly upregulated miRs are predicted to target the mRNAs of a number of matrisome proteins that are down-regulated in caNrf2 fibroblasts at both the RNA and protein levels (Fig. 4B). The members of the miR-29 family, which have previously been identified as Nrf2 targets in keratinocytes [35], and which are known to target ECM genes in fibroblasts [36], were only slightly elevated in caNrf2 fibroblasts (miR-seq) and showed no significant difference when examined using qRT-PCR (Table S1, Fig. S5B). This suggests cell type-specific differences in the regulation of miRs by Nrf2. However, other miRs were strongly regulated by caNrf2 in fibroblasts. Of these, miR-138-5p and miR-129-5p were selected for further study, since they were the most upregulated miRs that also have human orthologues. Strong overexpression of both miR-138-5p and miR-129-5p in caNrf2 fibroblasts was confirmed using qRT-PCR (Fig. 4C). Expression of these miRs was also upregulated in wild-type fibroblasts after a 24 h treatment with the Nrf2-activating compound tert-butylhydroquinone (tBHQ) (Fig. 4D). To investigate whether the genes encoding these miRs are direct transcriptional targets of Nrf2, genomic DNA upstream of the miR coding regions was examined for Nrf2 binding sites (AREs). For both miR-138-5p and miR-129-5p, stem-loops coding for their corresponding mature miR exist on two separate locations in the genome. miR sequencing results suggested that the bulk of miR-138-5p originated from the miR-138-1 stem-loop on chromosome 9, and miR-129-5p from the miR-129-2 stem-loop on chromosome 2 (Fig. S5C). Multiple AREs were identified upstream of the stem-loop sequences of all of the most strongly upregulated miRs, including miR-138-1 and miR-129-2, indicating that the genes encoding these miRs could be direct Nrf2 targets (Figs. 4E,F and S5D). Chromatin immunoprecipitation (ChIP) confirmed that Nrf2/caNrf2 indeed bind to these ARE sequences to a similar extent as to the ARE of the classical Nrf2 target gene NADP(H) quinone dehydrogenase 1 (*Nqo1*), and this was more pronounced in caNrf2 vs.

ctrl fibroblasts (Fig. 4G). Expression of miR-129-5p was also significantly elevated in the dermis of caNrf2 mice, while miR-138-5p showed little difference to control mice (Fig. 4H). This may be explained by the expression of miR-138-5p in other cell types of the dermis. Indeed, expression of *Nqo1* also showed little difference between genotypes, as its expression in other cells likely dilutes the expected increase in fibroblasts (Fig. 4H). To test this hypothesis, we mated caNrf2 mice with mice expressing green fluorescent protein (GFP) in fibroblasts and sorted the GFP-positive cells from newborn dermis. Expression of both miRs and of *Nqo1* was indeed significantly upregulated in GFP-positive cells of caNrf2 mice (Fig. 4H). *In situ* hybridization confirmed the *in vivo* expression of miR-138-5p and miR-129-5p in the vast majority of caNrf2 mouse dermal fibroblasts (Figs. 4I and S5E), but not in fibroblasts of ctrl mice (Fig. S5E). Taken together, these results show that Nrf2 regulates the expression of a multitude of miRs in skin fibroblasts *in vitro* and *in vivo*, and suggest that many of them are direct Nrf2 targets.

Nrf2-regulated miRs suppress collagen and elastin expression

To determine whether Nrf2-regulated miRs indeed suppress the expression of certain matrisome proteins, caNrf2 fibroblasts were treated with inhibitors (anti-miRs) against miR-138-5p and miR-129-5p. This caused a strong downregulation of these miRNAs (Fig. S6A), but the mRNA levels of the major skin collagens (*Col1a1*, *Col1a2* and *Col1a3*) failed to show significant increases (Fig. 5A). A likely explanation is that the large number of miRs upregulated upon activation of Nrf2 act collectively to suppress collagen expression, with a number of miRs able to compensate for the inhibition of a single miR. Indeed, analysis of all significantly upregulated miRs in caNrf2 fibroblasts showed that most of them are predicted to target one or more of the collagen mRNAs that are downregulated in caNrf2 fibroblasts (Fig. 5B). The potency of these miRs to suppress collagen expression was demonstrated when wild-type fibroblasts were transfected with individual mimics for miR-138-5p and miR-129-5p. Both miR mimics strongly reduced the mRNA levels for the

calculate the F-SHG/B-SHG ratio. $N = 6$ skin samples from different mice. Scale bars = 25 μm . (C) Analysis of collagen structure and pattern based on images collected using F-SHG. $N = 6$ skin samples from different mice. Values were obtained using the TWOMBLI plugin for ImageJ [18]. (D) Example image of back skin attached to the stretching apparatus. The part of the skin locally being examined is included in the red circle. (E–I) Quantification of the local stretch at peak tension before relaxation (0.1 N mm^{-1}) (E), tension change over time following initial stretch to peak tension (F), relative change in tension in response to changes in osmolarity (G), nominal tension at rupture (H), and local stretch at rupture (I). $N = 12\text{--}25$ skin samples from 3–5 mice per group. (J) “J-shaped” curves of nominal tension to stretch up to rupture. $N = 12\text{--}25$ skin samples from 3 to 5 mice per group. “J” curves represent the change in tension relative to the amount of stretch up to the point of rupture. $N = 12\text{--}25$ skin samples from 3 to 5 mice per group. Bar graphs show mean \pm s.e.m. Numbers above bars show exact p -values (Welch’s t -test). Significant differences are indicated in bold.

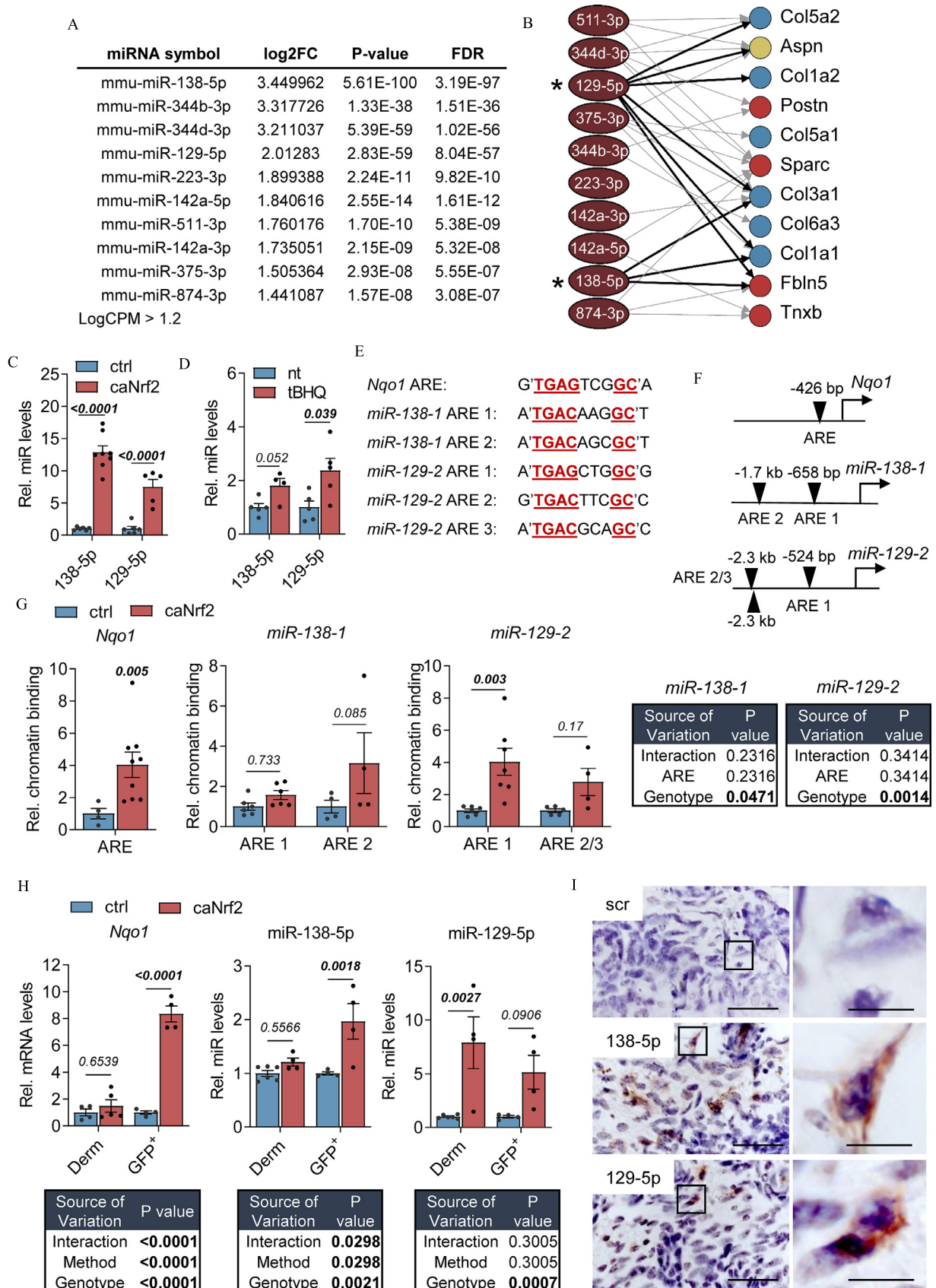


Fig. 4. *Nrf2* regulates collagen-targeting miRNAs in fibroblasts. (A) Top upregulated miRNAs in caNrf2 vs. ctrl fibroblasts identified by miR-seq, not including star sequences or miRNAs with LogCPM < 1.2. Full list is shown in Table S1. (B) Top 10

Nrf2-regulated miRs target collagen mRNAs

The production of collagen is heavily regulated by the differentiation of fibroblasts into myofibroblasts, which occurs for example during wound healing and when fibroblasts are isolated and cultured on a stiff surface [37]. We therefore examined whether the suppression of collagen via Nrf2-regulated miRs is a direct effect, or a result of inhibited myofibroblast differentiation. The morphology of cultured primary mouse skin fibroblasts was not affected by treatment with mimics of miR-138-5p or miR-129-5p, and in all cases, alpha smooth muscle actin (α -SMA) localized to stress fibers as is typical for differentiating fibroblasts in culture (Fig. 6A). The contractile ability of these cells, a characteristic trait of myofibroblasts, was not reduced upon treatment with mimics. In the case of miR-138-5p, collagen gel contraction was even mildly, but significantly promoted (Fig. 6B). Expression of the *Acta2* gene (encoding α -SMA) was also not reduced following treatment with miR mimics (Fig. 6C). Together, these results strongly suggest that miR-138-5p and miR-129-5p do not suppress ECM/collagen expression by inhibiting myofibroblast differentiation, but rather act by directly targeting collagen mRNAs.

To test this possibility, we examined the mRNAs of two major skin collagens that were most strongly downregulated following treatment with miR mimics: Col1 α 1 and Col3 α 1. Multiple miR binding sites were predicted in the 3'-UTR of the Col1 α 1 and Col3 α 1 mRNAs (DNA sequence shown in Fig. 6D,E and Table S2). We therefore transfected HEK 293T cells with a luciferase reporter plasmid encoding the full-length 3'-UTR of either Col1 α 1 or Col3 α 1. Cells transfected with any of these plasmids showed significantly lower luciferase activity upon co-transfection with miR-138-5p or miR-129-5p mimics compared to cells co-transfected with scrambled control (Fig. 6D–G). The effect of the miR mimics was abolished upon mutation of at least one of the predicted binding sites within the Col1 α 1 and Col3 α 1 3'-UTRs (Fig. 6D–G). These results confirm that both Nrf2-regulated miRs bind to the 3'-UTRs of collagen mRNAs, demonstrating that they directly regulate the expression of these collagens.

Aged human skin fibroblasts possess a matrisome similar to caNrf2 fibroblasts

To investigate the translational relevance of our findings, we determined how the aging matrisome in caNrf2 fibroblasts relates to what is observed in aged skin fibroblasts in humans. Therefore, we performed GSEA using published fibroblast datasets generated from different fibroblast subpopulations that were identified in aged human skin using single cell RNA-seq (Fig. 7A) [38]. Enrichment was observed for up- and downregulated genes in

certain fibroblast subpopulations, however the strongest enrichment was observed in 3 out of 4 fibroblast subpopulations when gene sets were filtered to include only matrisome genes (Fig. 7A). Examination of leading-edge genes again shows the downregulation of genes encoding skin collagens (e.g. *COL1A2*, *COL3A1*, *COL5A1*) as a primary feature of the matrisome in aged fibroblasts (Fig. 7A). Therefore, NRF2-mediated expression of the aging matrisome may further promote age-related changes in the majority of human fibroblasts, in particular when NRF2 gets activated by intrinsic or extrinsic cues, such as UVA irradiation [39].

To see if NRF2-regulated targeting of collagens by miRs is conserved in humans, we treated human fibroblasts with mimics for both miR-138-5p and miR-129-5p. Indeed, the mRNA levels of many of the major skin collagens were significantly reduced by this treatment (Fig. 7B). Furthermore, analysis of upregulated miRNAs in caNrf2 fibroblasts, most of which are conserved in humans, showed that many of these miRs are also predicted to target mRNAs for the major skin collagens in humans (Figs. 7C and S7).

NRF2 is activated in human skin fibroblasts upon aging

To more closely examine how aging affects NRF2 activity in fibroblasts in the context of the skin, we modelled human skin *in vitro* by generating skin equivalents with normal human dermal fibroblasts (NHDF) isolated from skin of old and young individuals together with normal human epidermal keratinocytes (NHEK). Staining of these skin equivalents with an antibody against phosphorylated NRF2, which detects activated NRF2 in the nucleus, showed a tendency towards stronger staining in nuclei of aged fibroblasts (Fig. 7D). To quantify the activity of NRF2 in these skin equivalents, we isolated RNA and analyzed the expression of four classical NRF2 target genes. The mRNA levels of *NQO1* and of glutamate cysteine ligase catalytic and modifier subunit (*GCLC* and *GCLM*) were indeed significantly higher in skin equivalents containing fibroblasts isolated from aged vs. young individuals, and expression of sulfiredoxin 1 (*SRXN1*) was also mildly elevated (Fig. 7E).

Finally, we examined sections from healthy human skin taken from individuals of different ages (sun-exposed head/neck area) for evidence of NRF2 activation. Immunohistochemical analysis of pNRF2 showed nuclear staining in dermal cells (i.e. mainly fibroblasts, excluding epidermis, hair follicles, vessels) in all samples with obvious interindividual differences. Importantly, however, the highest number of pNRF2-positive cells in the dermis was observed in skin from individuals 70 years of age and older, independent of the gender (Fig. 7F,G). These results challenge the view that NRF2 activity

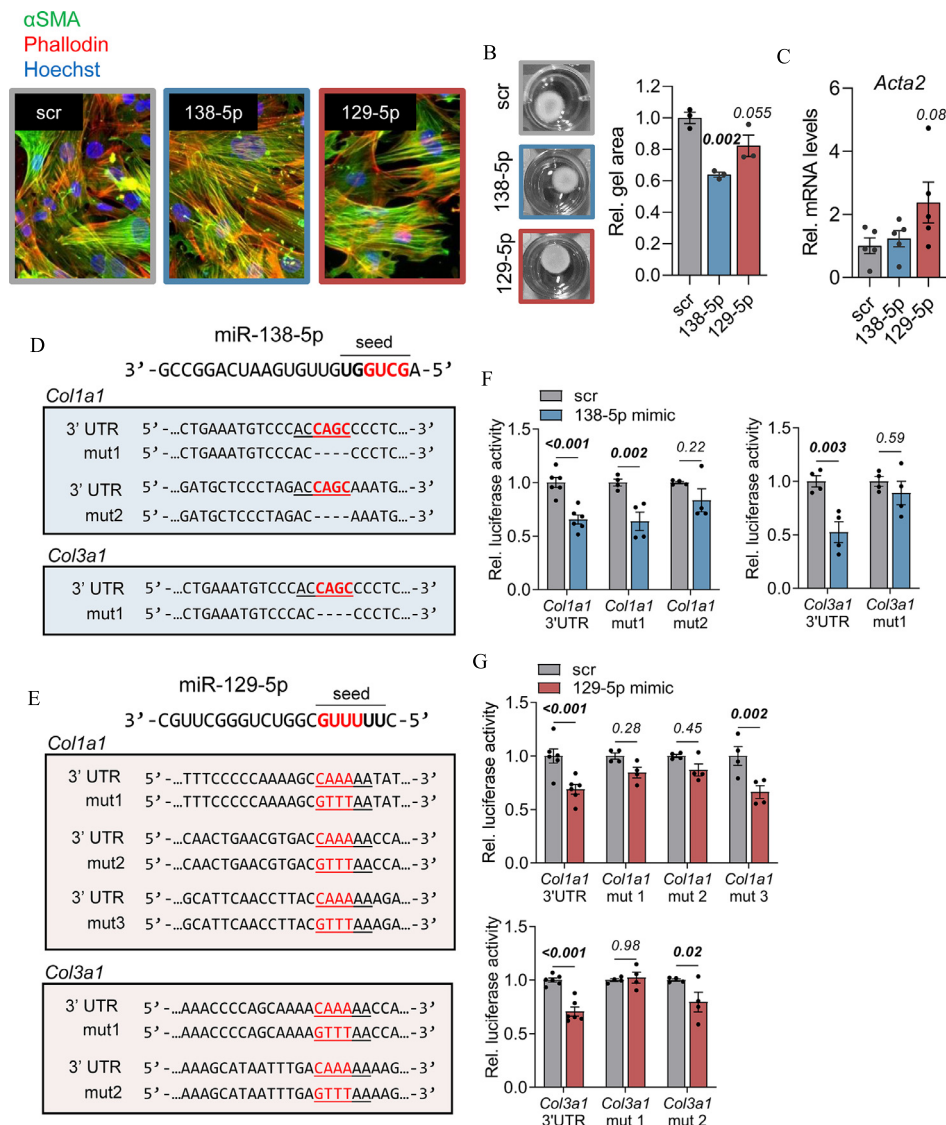


Fig. 6. Nrf2-regulated miRs directly suppress collagen expression. (A) Immunofluorescence staining of fibroblasts transfected with 138-5p and 129-5p miR mimics or scrambled (scr) control for α SMA (green), combined with phalloidin staining of the actin cytoskeleton (red) and Hoechst staining of nuclei (blue). (B) Collagen gel contraction by wild-type fibroblasts treated with miR mimics or scr control. $N = 3$ cell cultures from different mice. (C) qRT-PCR for *Acta2* using RNA from wild-type fibroblasts treated with miR mimics or scr control. $N = 4-5$ cell cultures from different mice. (D, E) 3'UTR of *Col1a1* and *Col3a1* with the miR binding sites in the corresponding mRNA and mutated sequences for (D) miR-138-5p and (E) miR-129-5p binding sites. Red bases indicate the mutated sequence in the 3'UTR and corresponding position within the miR seed sequence. (F, G) Results from dual luciferase assay using lysates of fibroblasts transfected with reporter constructs harboring the wild-type 3'UTR of *Col1a1* and *Col3a1* and mutated versions, following transfection with mimics of (F) miR-138-5p or (G) miR-129-5p or scr control. $N = 4-6$ transfections. Bar graphs show mean \pm s.e.m. Numbers above bars show exact p-values vs. scr (B, C: One-way ANOVA with Dunnett's multiple comparisons test, F, G: Two-way ANOVA with Sidák's multiple comparisons test). Significant differences are indicated in bold. Scale bars = 50 μ m.

necessarily declines with age, and even points to increased NRF2 activity in aged dermal fibroblasts. Therefore, NRF2 activation in skin, either through endogenous stimuli or via UVA-induced or pharmacological activation, may exacerbate age-related phenotypes in ECM production, organization and overall skin function.

Discussion

We discovered that Nrf2, which is mainly known for its role in the cellular redox homeostasis, regulates ECM synthesis in fibroblasts by direct transcriptional regulation of miR genes and corresponding upregulation of miRs. Nrf2-regulated miRs

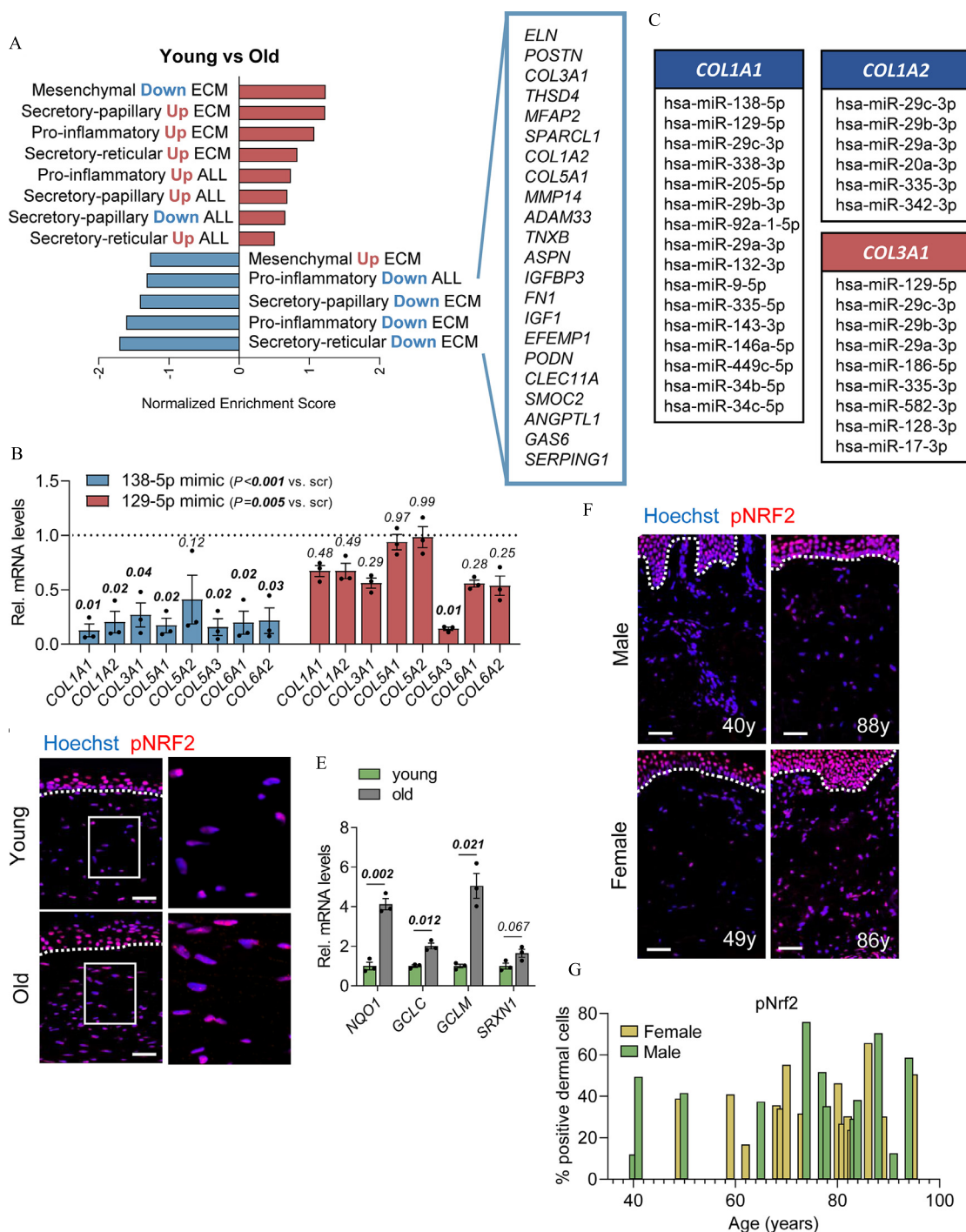


Fig. 7. Activation of NRF2 in fibroblasts of aged human skin. (A) Genes regulated in cultured caNrf2 vs. ctrl fibroblasts subjected to GSEA against gene sets from fibroblasts of different human fibroblast sub-populations in aged human skin *in vivo* [38]. Analyses are included for all differentially regulated genes and also for differentially regulated matrisome genes. Normalized enrichment score (NES) is shown along with nominal p value (P) and FDR q -value (FDR). (B) qRT-PCR for major skin collagens using RNA from human fibroblasts from 3 donors following treatment with miR mimics. (C) Lists of Nrf2-regulated miRNAs that are predicted to target human collagen mRNAs (TargetScan human). (D) Representative immunofluorescence images of pNRF2 on skin equivalents with fibroblasts from a young and an old human subject stained for pNRF2 using immunofluorescence (red). Nuclei were counterstained with Hoechst (blue). The area indicated with a white rectangle is shown at higher magnification on the right-hand side. (E) qRT-PCR for *NQO1*, *GCLC*, *GCLM*, *SRXN1* using RNA from skin equivalents with fibroblasts from young or old human subjects. $N = 3-4$ cultures. (F,G) Representative immunofluorescence images of pNRF2 on sections from healthy human skin of male and female subjects of different

directly suppressed the expression of the major skin collagens as well as certain proteoglycans and elastin in fibroblasts. This correlated with significant alterations in the biomechanical properties of the skin, and mimicked age-related skin phenotypes.

Many collagen-related factors have been shown to influence skin biomechanics, such as the total amount of collagen, the relative amounts of different collagens, the organization of collagen fibers, their re-organization under mechanical loading, and the degree of collagen cross-linking [40–42]. This is highlighted in hypertrophic scars, which display different stiffness and strength associated with altered collagen content, a different proportion of various collagens, and altered collagen organization when compared to healthy skin [43,44]. In the present work, we show that the total amount and microstructure of collagen is altered in caNrf2 skin and interpret this as the main cause of biomechanical differences between the two types of skin, since it is in line with the existing understanding of collagenous tissue biomechanics [43,44].

Recent results have unraveled a role for Nrf2 in regulating the ECM [45]. This effect can be indirect through suppression of ROS levels, but direct transcriptional activation of certain matrix genes by Nrf2 has also been demonstrated [16]. While early experiments using *Keap1* knockout mice showed that Nrf2 can regulate the expression of genes in keratinocytes that code for proteins of the cornified envelope [46], which is considered as a special type of ECM [47], our findings show that Nrf2 regulates major ECM genes that are characteristic for dermal/connective tissue, in particular collagens. Traditionally, the connection between Nrf2 and ECM synthesis has largely been viewed in the context of fibrosis and ROS-mediated transforming growth factor- β signaling [48]. Indeed, reduced Nrf2 activity and the resulting redox imbalance have been observed in fibrosis of multiple organs, and restoration of redox balance is considered a priority for prevention or resolution of this pathology [48,49]. This has been demonstrated, for example, for the autoimmune disease systemic sclerosis (SSc), which results in fibrosis of skin and internal organs. Reduced expression and activity of NRF2 was detected in skin fibroblasts from SSc patients and from an SSc mouse model [50]. Furthermore, the fibrotic phenotype in this model aggravated in an *Nrf2* knockout background [50]. While we did not observe obvious macroscopic differences in internal organs from caNrf2 mice, the expression of caNrf2 in mesenchymal cells may

have important consequences for these organs as well, particularly under pro-fibrotic conditions. This important aspect should be addressed in future studies. While the loss of Nrf2 promotes fibrosis, our previous work has shown that Nrf2 activation in fibroblasts reduces scarring following skin wounding [16]. This is likely the consequence of the miRNA-dependent down-regulation of collagens identified in the present study.

While the anti-fibrotic effect of Nrf2 activation is beneficial, our results show that Nrf2 regulation of the ECM impairs the biomechanical properties of the skin. Skin tearing in the elderly is a significant clinical problem, and can even lead to chronic wounds [51]. When compared to ctrl mice, caNrf2 mouse skin toughness was reduced, with no progressive resistance to deformation associated with over-physiological stretch. Therefore, much less force was required for tissue rupture, a finding that was closely mimicked in old wild-type mice. Interestingly, skin stiffness in the physiological deformation range was not impaired. This indicates that, despite the impact on tissue microstructure demonstrated by loading to over-physiological stretch, there are compensating mechanisms ensuring fulfilment of biomechanical function for physiological deformations. The reduced response of skin from young caNrf2 mice and aged wild-type mice to altered osmolarity may be indicative of lower fixed charge density, since the negative charges of glycosaminoglycans play a key role in water retention. The latter is obviously important for skin hydration, and lower skin hydration is a clinical characteristic of skin aging [9].

Our results suggest that altered collagen deposition and ECM organization during pro- and postnatal development in caNrf2 mice likely have important functional consequences later in life. Therefore, prolonged activation of Nrf2 in fibroblasts can accelerate certain aspects of the aging process. This is not restricted to the reduction in collagen and elastin expression, but also includes the induction of cellular senescence, which we observed in caNrf2 fibroblasts *in vitro* and *in vivo* [16] and which is a hallmark of aged skin [52,53]. Senescent cells produce a senescence-associated secretome, which includes a variety of pro-inflammatory cytokines, and can result in enhanced or chronic inflammation [54]. Indeed, caNrf2 mice have more immune cells in normal skin already at 10 weeks of age [16]. Aged skin is also more prone to malignant transformation as seen by the strong skin cancer incidence in aged individuals [55]. While multiple factors are likely to

ages (F) and quantification of the percentage of stained area within the dermis – excluding cells within hair follicles and large vessels. (G). Bar graphs show mean \pm s.e.m. Numbers above bars show exact *p*-values (Two-way ANOVA with Sidák's multiple comparisons test (B) and Welch's *t*-test (E)). Numbers (B) next to 138-5p mimic and 129-5p mimic show *p*-values for specific mimic vs. scr for all collagen genes grouped. Significant differences are indicated in bold. Scale bars = 50 μ m.

contribute to this effect, Nrf2 expression/activity in aged skin may well play a role, since constitutive Nrf2 activation in skin fibroblasts promoted a cancer-associated fibroblast phenotype [16]. Finally, wounds in aged individuals frequently heal with less scarring compared to wounds in young patients [56], a phenomenon also observed in old wild-type mice [57] and in caNrf2 mice [16]. Consistent with these findings, our new results suggest that NRF2 activity in human skin fibroblasts frequently increases with advanced age, which likely contributes to these age-related alterations. The increased NRF2 activation in aged human skin may be a consequence of frequent UV exposure, because UVA is known to activate NRF2 in fibroblasts [39]. Consistent with this assumption, most human skin samples that we obtained were from sun-exposed skin.

Overall, the results presented here challenge the dogma that Nrf2 acts exclusively as an anti-aging factor in mammals. While it is well established that even the basal activity of Nrf2 plays a central role in controlling the accumulation of excessive ROS that may occur over time [10] and thereby limits UV-induced photoaging [58], our data suggest that chronic activation of Nrf2 in fibroblasts via the resulting matrix alterations may have adverse effects in skin worth considering as it pertains to skin aging.

While the phenotype observed in the caNrf2 transgenic mice is a consequence of long-term activation of Nrf2-mediated gene expression already during development, the rapid down-regulation of collagen expression in cultured fibroblasts by NRF2-activating compounds suggests that short-term activation of NRF2 may already affect the ECM. This has direct consequences for the use of NRF2 activating compounds *in vivo*. Such compounds have shown promise in different diseases [6], but there are also important downsides to NRF2 activation in skin and other organs [59–61]. Therefore, it is important to understand the mechanisms and cell types involved in order to best discern under what circumstances NRF2 activation might be beneficial or detrimental. Our study provides an important example for the double-edged sword of NRF2 activation by uncovering previously unknown mechanisms of ECM regulation in fibroblasts. These effects may be beneficial in some cases (e.g. fibrosis prevention), but may also have detrimental effects on skin biomechanics and aging. Therefore, pharmacological activation of NRF2 in the skin should be performed with these findings in mind. Finally, our results identify an unexpected role of long-term NRF2 activation in exacerbating certain aspects of skin aging and raise the interesting question if a moderate reduction of NRF2 activity in the skin, e.g. using chemical inhibitors [62], may slow down the aging process in this organ or even revert it in aged patients.

Experimental procedures

Additional details regarding antibodies, primer sequences and reagents used in this study are listed in Table S3.

In vivo mouse experiments

Mice were housed and fed according to Swiss federal guidelines. Male Col1a2Cre mice in C57BL/6 background [63] were mated with CMVcaNrf2 mice (FVB/N background) [13] to generate mice expressing caNrf2 in mesenchymal cells [16]. Only progeny of the F1 generation were used for experiments. To generate triple transgenic mice containing the PDGFR α -eGFP transgene (mice that express a H2B-eGFP fusion gene from the endogenous *Pdgfra* locus [64]), Col1a2Cre hemizygous mice were first bred with PDGFR α -eGFP hemizygous mice to generate double transgenic progeny, which were then used for breeding with CMVcaNrf2 mice. Old mice (20 months) and young control mice (10 weeks) in (C57BL/6JRj) genetic background were purchased from Janvier Labs (Le Genest Saint Isle, France). Male/female comparison of Col1a2Cre-CMVcaNrf2 mice was performed previously [16] and in this study, male mice were used to generate sufficient sample sizes due to a slight increase in weight. To genotype the mice, DNA from ear biopsies was amplified by PCR using the KAPA2G FAST Genotyping Mix (Roche, Rotkreuz, Switzerland). All animal experiments were performed in the morning. Mouse maintenance and animal experiments had been approved by the local veterinary authorities (Kantonales Veterinäramt Zürich).

Human skin samples

Human skin, which was removed upon surgery, e.g. of an adjacent benign or malignant skin lesion, was obtained anonymously from the Department of Dermatology, University Hospital Zurich, in the context of the biobank project. Use of the samples was approved by the local and cantonal Research Ethics Committees. Informed consent for research was obtained before routine diagnostic services. Most samples were from sun-exposed areas of the skin.

Isolation and culture of primary dermal fibroblasts

Fibroblasts were isolated from skin of P1.5 mice. The sex of these newborn mice is unknown. Dermis was separated from epidermis by incubation in trypsin/EDTA (5%) for 1 h at 37 °C, followed by peeling off the epidermis. The dermis was minced into small pieces and incubated with a collagenase type II solution (2.5 ml, 500 U ml⁻¹; Worthington Biochemical Corporation, Lakewood, NJ) for 1 h at 37 °C with

manual agitation every 15 min. The cell suspension was poured through a 100 μm cell strainer and centrifuged at 1200 rpm for 5 min. The resulting pellet was re-suspended in DMEM (8 ml, Sigma, Munich, Germany; D6429)/10% fetal bovine serum (FBS)/penicillin/streptomycin and the cells were seeded into two 6 cm dishes. Medium was changed the following day and cells were passaged prior to confluency.

Immunofluorescence analysis of cultured fibroblasts

Ctrl and *caNrf2* fibroblasts at passage 2 were fixed for 10 min in paraformaldehyde (4%) and treated with bovine serum albumin (BSA, 1%, Sigma) for 10 min. Fixed cells were incubated with an antibody against αSMA (Sigma; A2547) and an Alexa Fluor 488-coupled secondary antibody (Jackson ImmunoResearch, Waltham, MA; 715-545-150). The actin cytoskeleton was stained with rhodamine-coupled phalloidin, and nuclei were counterstained with Hoechst 33342.

Histology, immunohistochemistry and immunofluorescence staining

Skin samples were fixed in phosphate buffered formaldehyde (4%) solution for 24 h at room temperature (RT), processed, and embedded in paraffin (mouse and human) or directly frozen in tissue freezing medium[®] (mouse) (Leica Biosystems, Nussloch, Germany). Sections (7 μm) were stained using hematoxylin & eosin or Sirius Red. Analysis of Picrosirius Red stained sections was performed using ImagePro Plus (Media Cybernetics Inc., Rockville, MD) for color segmentation, and the TWOMBLI plugin for ImageJ to examine the ECM pattern [18]. Analysis of fiber orientation was done using OrientationJ [19]. For pNRF2 immunofluorescence analysis, paraffin sections were dewaxed and rehydrated using a xylene/ethanol gradient followed by antigen retrieval using citrate buffer (pH 6.0) at 95 °C for 1 h. Sections were incubated with antibodies against pNRF2 (Abcam, Cambridge, UK; ab76026) at a dilution of 1:500 in BSA (12%) overnight at 4 °C. For collagen I immunofluorescence analysis, fresh frozen sections were fixed with ice-cold acetone for 10 min and treated with antibodies against collagen I (Southern Biotech, Birmingham, AL; 1310-01) at a 1:400 dilution in BSA (1%) overnight at 4 °C. pNRF2 immunofluorescence was visualized using anti-rabbit Cy3 (Jackson ImmunoResearch; 111-165-003) at a 1:400 dilution in BSA (12%), and collagen I immunofluorescence was visualized using anti-goat AlexaFluor 488 (Jackson ImmunoResearch; 705-545-003) at a 1:500 dilution in BSA (1%).

In situ hybridization

Formalin-fixed, paraffin-embedded skin sections were de-waxed and rehydrated using RNase-free water. Sections were then treated with proteinase K (100 $\mu\text{g/ml}$) for 15 min at 37 °C and then washed twice in RNase-free water. For hybridization, digoxigenin (DIG)-labelled probe (6 pmol, miRCURY LNA miRNA Detection Probe, Qiagen, Hilden, Germany; 339111) was incubated at 55 °C for 3 h. Sections were then washed in decreasing concentrations of saline-sodium citrate (SSC) followed by RNase-free PBS. They were then treated with blocking solution (1% BSA), followed by immunohistochemistry/immunofluorescence staining using a goat anti-DIG antibody (Abcam; ab76907 at 1:500 dilution in BSA (1%) overnight at 4 °C), followed by a biotinylated anti-goat secondary antibody (Jackson ImmunoResearch; 705-065-003, 1:500 dilution in 1% BSA). For histochemical visualization, we used the Vectastain ABC kit (Vector Laboratories, Burlingame, CA; PK-6100) and the DAB peroxidase substrate kit (Vector Laboratories; SK-4100). Alternatively, fluorescence was visualized using Alexa Fluor[™] 594 Tyramide SuperBoost[™] Kit (Thermo Fisher Scientific, Waltham, MA; B40935).

RNA isolation and qRT-PCR

RNA was isolated from cultured fibroblasts using Trizol[®] according to the manufacturer's instructions (Life Technologies, Carlsbad, CA; # 15596,) and reverse transcribed using the iScript[™] cDNA synthesis kit (BioRad, Hercules, CA; # 1708890). Quantitative PCR was performed using a LightCycler[®] 480 SYBR Green I Master reaction mix (Roche, Rotkreuz, Switzerland). Data was quantified using second derivative maximum analysis and gene expression represented as relative to the house-keeping genes *Rps29* (for mouse genes) or *RPL27* (for human genes).

RNA isolation from skin equivalents

Frozen skin equivalents were homogenized by adding zirconium beads and shaking in a tissue homogenizer (Precellys24, Bertin Instruments, Montigny-le-Bretonneux, France) twice for 15 s at 5000 rpm. RNA was isolated using the InnuPrep DNA/RNA Mini Kit (Jena Analytik, Jena, Germany) according to the manufacturer's instructions.

Fluorescence-activated cell sorting for RNA isolation

Mice expressing the H2B-eGFP fusion protein (with or without the *caNrf2* transgene) were sacrificed. Skin was removed from the back of newborn

(P2.5) mice, minced into small pieces, followed by incubation in 2 ml of medium containing Liberase TL (0.25 mg ml⁻¹, Roche), DNase I (0.25 mg ml⁻¹, Sigma), and MgCl₂ (7.5 mM) for 1 h at 37 °C while shaking at 100 rpm. The cell suspension was passed through a 70 μm cell strainer and washed with PBS containing DNase I (0.25 mg/ml) and MgCl₂ (7.5 mM). Cells were centrifuged for 10 min at 1200 rpm and resuspended in FACS buffer (0.5% BSA, 5 mM EDTA in 1 × PBS). To exclude non-viable cells, Sytox Red (1:1000; Invitrogen, Carlsbad, CA) was used according to the manufacturer's instructions. Cells were sorted using the BD FACSAria Illu equipped with FACSDiva software version 6 (BD Pharmingen, San Diego, CA). eGFP⁺ cells were sorted into RNase-free 1.5 ml tubes with FACS buffer (100 μl) supplemented with RiboLock RNase Inhibitor (Thermo Fisher Scientific) at 10 U per sample.

miRNA real-time PCR and miR-sequencing

Analysis of miRNAs was done using total RNA isolated as described above. Total RNA was diluted and miRNAs were reverse transcribed into cDNA using the TaqManTM Advanced miRNA cDNA Synthesis Kit (Thermo Fisher Scientific; A28007) according to the manufacturer's instructions. Real-time PCR was performed using TaqMan[®] Universal Master Mix II (no UNG) (Thermo Fisher Scientific; 4440040) and TaqManTM Advanced miRNA Assays (Thermo Fisher Scientific; A25576) for miR-138-5p (477905_mir) and miR-129-5p (480913_mir). miR-191-5p (477952_mir) was used as a housekeeping miR for normalization. For miR sequencing, primary fibroblasts from three different mice per genotype (ctrl and caNrf2) were used. Fibroblasts were allowed to proliferate in culture for 6 d to allow for sufficient numbers for miRNA sequencing at passage 1. Total RNA was isolated from cells followed by miRNA-seq analysis. RNA quality was determined with a Qubit[®] (1.0) Fluorometer (Life Technologies, Carlsbad, CA) and a Bioanalyzer 2100 (Agilent Technologies, Santa Clara, CA). Only samples with a 260 nm/280 nm ratio between 1.8 and 2.1 and a 28S/18S ratio within 1.5–2 were further processed. Small RNA libraries were prepared for sequencing using standard Illumina protocols, and sequencing was performed on the Illumina HiSeq 2500. Base calling was performed with CASAVA v.1.8, and further data processing including differential expression analysis was performed using the miARma-seq tool and accompanying software [65]. The miR-seq data have been deposited at NCBI's Gene Expression Omnibus [66] (GSE180484) and are publicly available as of the date of publication.

Transfection of fibroblasts with anti-miRs or miR mimics

Fibroblasts were ~50% confluent at the time of transfection with mimics or anti-miRs (final concentration 3.75 nM). Lipofectamine RNAiMAX Transfection Reagent (13778150, Thermo Fisher Scientific) was diluted in reduced serum medium (7.5 μl per 125 μl of OptiMEM), mixed with diluted miR mimic or miR inhibitor and incubated at room temperature for 10 min. The mixture was then added dropwise to individual wells of a 6-well plate containing 2 ml of media (250 μl per well). Cells were maintained for 72 h and homogenized using Trizol.

Luciferase reporter assays

miRNA 3'-UTR dual luciferase plasmids were from GeneCopoeia Rockville, MA (Col3a1 3'-UTR: MmiT067266-MT06 and Col1a1 3'-UTR: MmiT091572-MT06). 3'-UTR sequences are shown in Table S2. Human embryonic kidney (HEK) 293T cells were grown to ~50% confluency and transfected with miR mimics (50 nM final concentration) and luciferase plasmids (0.5 μg/ml). Lipofectamine 2000 Transfection Reagent (11,668, Thermo Fisher Scientific) was diluted in reduced serum medium (OptiMEM, 0.6 μl per 16 μl of OptiMEM), mixed with diluted miR mimics/plasmids and incubated at room temperature for 10 min. The mixture was then added dropwise to individual wells of a 48-well plate containing 250 μl of medium (32 μl per well). Cells were maintained for 24 h, and firefly/renilla luciferase activities were measured using the Dual Glo Luciferase Assay System (Promega, Madison, WI; E2920).

Human skin equivalents

Normal human dermal fibroblasts (NHDF) and normal human epidermal keratinocytes (NHEK) were isolated from human skin samples as previously described [67]. Keratinocytes were propagated in FAD/10% FBS/penicillin/streptomycin at 37 °C, 5% CO₂, and 20% O₂ and fibroblasts in DMEM/10% FBS/penicillin/streptomycin at 37 °C, 5% CO₂, 10% O₂. All cells in culture were regularly checked for mycoplasma contamination using the Venor[®]GeM OneStep Mycoplasma Detection Kit (Minerva Biolabs, Berlin, Germany).

Skin equivalents were generated using methods previously described [68]. Briefly, NHDF derived from either young (22 y and 23 y) or old (66 y and 74 y) donors were seeded onto filter inserts with 0.4 μm pore size in 12-well deep-well plates (ThinCert[®], Greiner Bio-One, St. Gallen, Switzerland) in three successive steps. During a five-week submersed cultivation period, NHDF produce all components of the dermal ECM and build the dermal equivalent. NHEK were seeded on top of the dermal equivalent

and were subsequently cultured at the air-liquid interphase to initiate the generation of a stratified, well differentiated epidermis.

Biomechanical analysis of mouse skin

Experiments were based on methods described previously [69]. After sacrifice, the back skin of adult mice (10 weeks of age) was shaved, marked to identify the cranial end, and removed to obtain a piece of skin of approximately 6 × 3 cm (adult) or 3 × 2 cm (newborn) suitable for biomechanical analysis. Any visible loose fat tissue was dissected. Skin was kept flat in cold DMEM on ice, and mechanical experiments were performed on the same day.

Skin samples, 40 mm × 5 mm (10-week-old and 20-month-old mice) and 20 mm × 2.5 mm (1-week-old mice), were cut parallel to the cranial-caudal direction using parallel razor blades. Samples were then clamped at either end using custom-made clamps, leaving 20 mm (10-week-old and 20-month-old mice) or 10 mm (1-week-old mice) free length, and loaded into a custom-built mechanical testing system (MTS Systems, Eden Prairie, MN) equipped with hydraulically actuated axes and force sensors (capacity of up to 20 N). During mechanical testing, each sample was imaged top-down with a CCD camera (Pike F-100B, Allied Vision Technologies GmbH, Stadroda, Germany) with a 0.25x telecentric lens (NT55-349, Edmund Optics Ltd., York, UK) at a rate of 4 Hz, while force and displacement data was recorded at 10 Hz. All samples were tested immersed in a 0.9% NaCl solution (Sigma) at room temperature.

Each sample was stretched longitudinally at a strain rate of 0.025/s⁻¹ until a predetermined peak force level was reached (0.5 N, leading in both cases to a nominal membrane tension – i.e. force divided by the nominal sample width – of 0.1 N/mm), after which the displacement was held constant for 10 min and force was measured as the sample relaxed (Movie S1). For experiments involving effects of hyper-/hypotonicity, the saline solution was drained after 1 min of relaxation and replaced with distilled water or NaCl (3.6%) to obtain a hypotonic or hypertonic solution, respectively. At least one sample per animal was tested for each tonicity condition and at least 3 samples per animal in total. After the relaxation period, the sample was unloaded and immediately loaded again at a strain rate of 0.025/s until rupture.

For analysis purposes, a reference configuration was defined when the measured force reached 0.02 N to ensure there was no slack in the sample. A custom optical flow tracking algorithm was used to extract strain information from the center of each sample during the whole experiment, as previously described [69,70]. For hyper-/hypotonic conditions, the relative change in tension ΔT at the end of the

relaxation phase was calculated relative to the average tension in the isotonic (0.9% NaCl) condition for each group as follows:

$$\Delta T = \frac{T_{\text{hyper or hypotonic}} - T_{\text{average, isotonic}}}{T_{\text{average, isotonic}}}$$

Gene ontology (GO) and gene set enrichment analysis (GSEA)

Examination of GO for leading edge genes was performed using Enrichr [71] or Revigo [72] to summarize GO terms that were enriched in the caNrf2 fibroblast dataset. For GSEA, sets of significantly up- or down-regulated genes were generated by re-analysing published sequencing data of skin fibroblasts from old and young subjects [25,38]. Original gene sets were uploaded to the WEB-based GENE SeT AnaLysis Toolkit (WebGestalt) and used for GSEA [73]. The datasets and samples analysed as well as methods for obtaining the gene sets are listed in Table S4 (mouse) and Table S5 (human). Original and filtered gene sets, ranked gene lists, and original GSEA output data for all experiments are also provided.

Chromatin immunoprecipitation (ChIP)

ChIP was performed exactly as previously described [16]. The following antibodies were used for IP: anti-histone H3 (Abcam; ab1791), anti-Nrf2 (Santa Cruz, Santa Cruz, CA; sc-722X), anti-Nrf2 (Thermo Fisher Scientific; PA5-27882), and anti-rabbit IgG (Merck Millipore, Burlington, MA; 12-370).

Multiphoton microscopy

Multiphoton microscopy and SHG imaging were performed on 30 μm thick skin sections using a Leica TCS SP8 microscope equipped with a 40 × 1.1 numerical aperture L Water HC PL IRAPO objective and a Mai Tai XF (Spectra-Physics, Milpitas, CA) MP laser tunable from 710 to 950 nm. F-SHG images were collected through an aligned condenser (0.55NA), SHG filter (435–455 nm) and PMT, while B-SHG signal was collected with internal HyD1 detector via open PH in the same spectral range as F-SHG as well as with an external non-descanned detector (HyD7) right after the objective (also 435–455 nm). Laser power was kept constant throughout each experiment, as were photomultiplier tube (PMT) voltage and gain. Leica SP8 LAS X v.3.5.5 software was used to control the instrument and for image acquisition. Image analysis was performed using ImageJ (National Institutes of Health, Bethesda, MD).

Determination of skin collagen content

Skin collagen content was determined using the QuickZyme Total collagen Assay Kit (QuickZyme Biosciences, Leiden, NL; QZBtotcol). Measurements were done using two 5 mm diameter skin biopsies taken from the back of the same mouse. Skin was first weighed and hydrolyzed using 6 M HCl for 20 h at 90 °C (50 mg/ml) and then analyzed according to the manufacturer's instructions.

Quantification and statistical analysis

Appropriate statistical testing was performed using GraphPad Prism software (GraphPad, San Diego, CA). Details of sample size and specific statistical test used are found in the figure legends. All *p*-values below 0.05 are considered significant and are labelled in bold within the figures. Numerical *p*-values for all statistical tests are shown.

CRedit authorship contribution statement

Paul Hiebert: Conceptualization, Data curation, Formal analysis, Funding acquisition, Investigation, Methodology, Validation, Visualization, Writing – original draft. **Anastasiya Martyts:** Formal analysis, Investigation, Validation, Visualization, Writing – review & editing. **Jonas Schwestermann:** Investigation, Validation, Writing – review & editing. **Katharina Janke:** Investigation, Validation, Writing – review & editing. **Jürg Hafner:** Investigation, Resources, Writing – review & editing. **Petra Boukamp:** Funding acquisition, Resources, Supervision, Writing – review & editing. **Edoardo Mazza:** Funding acquisition, Methodology, Software, Supervision, Writing – review & editing. **Sabine Werner:** Conceptualization, Funding acquisition, Project administration, Supervision, Writing – original draft.

Data Availability

Original data will be made available on request.

CRedit authorship contribution statement

Paul Hiebert: Conceptualization, Data curation, Formal analysis, Funding acquisition, Investigation, Methodology, Validation, Visualization, Writing – original draft. **Anastasiya Martyts:** Formal analysis, Investigation, Validation, Visualization, Writing –

review & editing. **Jonas Schwestermann:** Investigation, Validation, Writing – review & editing. **Katharina Janke:** Investigation, Validation, Writing – review & editing. **Jürg Hafner:** Investigation, Resources, Writing – review & editing. **Petra Boukamp:** Funding acquisition, Resources, Supervision, Writing – review & editing. **Edoardo Mazza:** Funding acquisition, Methodology, Software, Supervision, Writing – review & editing. **Sabine Werner:** Conceptualization, Funding acquisition, Project administration, Supervision, Writing – original draft.

Acknowledgments

We thank Christiane Born-Berclaz for excellent technical assistance, Dr. Peter Angel, German Cancer Research Institute, Heidelberg Germany for the Col2a2-Cre mice, Dr. Svitlana Kurinna, University of Manchester, for helpful suggestions with the miRNA experiments, and Dr. Gaetana Restivo, University Hospital Zurich, for help obtaining human samples. This work was supported by grants from the ETH Zurich (Career Seed Grant No. SEED-03 19-1 to PH), the SKINTEGRITY.CH Open ETH Project (to SW, JH and EM), the Swiss National Science Foundation (grants 31003A_169204 and 31003B-189364 to SW and 205321_179012 to EM), a Banting Postdoctoral Fellowship (to PH) and the BMBF project KAU VIR 02NUK036A (to PB).

Supplementary materials

Supplementary material associated with this article can be found in the online version at [doi:10.1016/j.matbio.2022.09.002](https://doi.org/10.1016/j.matbio.2022.09.002).

Received 11 July 2022;

Received in revised form 8 September 2022;

Accepted 12 September 2022

Available online 20 September 2022

Keywords:

Aging;
Skin mechanics;
Extracellular matrix;
Nrf2;
miRNA;
Collagen

Abbreviations:

ARE, antioxidant response element; B-SHG, backward SHG; caNrf2, constitutively active Nrf2; CDDO-Im, 1[2-Cyano-3,12-dioxooleana-1,9(11)-dien-28-oyl]imidazole; ChIP, chromatin immunoprecipitation; ctrl, control; F-SHG, forward SHG; GCLC, glutamate cysteine ligase catalytic

subunit; GCLM, glutamate cysteine ligase modifier subunit; GFP, green fluorescent protein; GSEA, gene set enrichment analysis; miRNA, miR, microRNA; miR-seq, miR sequencing; MMP, matrix metalloproteinase; NES, normalized enrichment score; NHDF, normal human dermal fibroblasts; NHEK, normal human epidermal keratinocytes; NQO1, NADP(H) quinone dehydrogenase 1; NRF2, nuclear factor erythroid 2-related factor 2 (mouse); NRF2, nuclear factor erythroid 2-related factor 2 (human); P2.5, postnatal day 2.5; SHG, second harmonic generation; qRT-PCR, quantitative real time PCR; RNA-seq, RNA sequencing; ROS, reactive oxygen species; SMA, smooth muscle actin; SSc, systemic sclerosis; SRXN1, sulfiredoxin 1; tBHQ, tert-butyl hydroquinone; TIMP, tissue inhibitor of metalloproteinases; 3'-UTR, 3'-untranslated region

References

- [1] K. Taguchi, H. Motohashi, M. Yamamoto, Molecular mechanisms of the Keap1-Nrf2 pathway in stress response and cancer evolution, *Genes Cells* 16 (2) (2011) 123–140.
- [2] E. Kansanen, S.M. Kuosmanen, H. Leinonen, A.L. Levenon, The Keap1-Nrf2 pathway: mechanisms of activation and dysregulation in cancer, *Redox Biol.* 1 (2013) 45–49.
- [3] G.P. Sykiotis, D. Bohmann, Stress-activated cap'n'collar transcription factors in aging and human disease, *Sci. Signal.* 3 (112) (2010) re3.
- [4] L. Baird, M. Yamamoto, The molecular mechanisms regulating the Keap1-Nrf2 pathway, *Mol. Cell. Biol.* 40 (13) (2020) e00099–20.
- [5] T. Suzuki, M. Yamamoto, Stress-sensing mechanisms and the physiological roles of the Keap1-Nrf2 system during cellular stress, *J. Biol. Chem.* 292 (41) (2017) 16817–16824.
- [6] A. Cuadrado, A.I. Rojo, G. Wells, J.D. Hayes, S.P. Cousin, W.L. Rumsey, O.C. Attucks, S. Franklin, A.L. Levenon, T.W. Kensler, A.T. Dinkova-Kostova, Therapeutic targeting of the Nrf2 and Keap1 partnership in chronic diseases, *Nat. Rev. Drug Discov.* 18 (4) (2019) 295–317.
- [7] Y. Gu, J. Han, C. Jiang, Y. Zhang, Biomarkers, oxidative stress and autophagy in skin aging, *Ageing Res. Rev.* 59 (2020) 101036.
- [8] C.T. Madreiter-Sokolowski, C. Thomas, M. Ristow, Interrelation between ROS and Ca(2+) in aging and age-related diseases, *Redox Biol.* 36 (2020) 101678.
- [9] G. Limbert, D. Pond, A. McBride, Constitutive modelling of skin ageing, *Stud. Mechanobiol. Tissue* 22 (2019) 135–192.
- [10] C.J. Schmidlin, M.B. Dodson, L. Madhavan, D.D. Zhang, Redox regulation by Nrf2 in aging and disease, *Free Radic. Biol. Med.* 134 (2019) 702–707.
- [11] D.R. Bruns, J.C. Drake, L.M. Biela, F.F. Peelor, B.F. Miller, K.L. Hamilton, Nrf2 signaling and the slowed aging phenotype: evidence from long-lived models, *Oxidative Med. Cell. Longev.* 2015 (2015) 732596.
- [12] M. Schafer, S. Dutsch, U.A.D. Keller, F. Navid, A. Schwarz, D.A. Johnson, J.A. Johnson, S. Werner, Nrf2 establishes a glutathione-mediated gradient of UVB cytoprotection in the epidermis, *Genes Dev.* 24 (10) (2010) 1045–1058.
- [13] M. Schafer, H. Farwanah, A.H. Willrodt, A.J. Huebner, K. Sandhoff, D. Roop, D. Hohl, W. Bloch, S. Werner, Nrf2 links epidermal barrier function with antioxidant defense, *EMBO Mol. Med.* 4 (5) (2012) 364–379.
- [14] U.A. Kohler, F. Bohm, F. Rolfs, M. Egger, T. Hornemann, M. Pasparakis, A. Weber, S. Werner, NF-kappaB/RelA and Nrf2 cooperate to maintain hepatocyte integrity and to prevent development of hepatocellular adenoma, *J. Hepatol.* 64 (1) (2016) 94–102.
- [15] L.Y. Lee, C. Harberg, K.A. Matkowskyj, S. Cook, D. Roenneburg, S. Werner, J. Johnson, D.P. Foley, Overactivation of the nuclear factor (erythroid-derived 2)-like 2-antioxidant response element pathway in hepatocytes decreases hepatic ischemia/reperfusion injury in mice, *Liver Transpl.* 22 (1) (2016) 91–102.
- [16] P. Hiebert, M.S. Wietecha, M. Cangkruma, E. Haertel, E. Mavrogonatou, M. Stumpe, H. Steenbock, S. Grossi, H.D. Beer, P. Angel, J. Brinckmann, D. Kleitsas, J. Dengjel, S. Werner, Nrf2-mediated fibroblast reprogramming drives cellular senescence by targeting the matrisome, *Dev. Cell* 46 (2) (2018) 145–161 e10.
- [17] L. Rittie, G.J. Fisher, Natural and sun-induced aging of human skin, *Cold Spring Harb. Perspect. Med.* 5 (1) (2015) a015370.
- [18] E. Wershof, D. Park, D.J. Barry, R.P. Jenkins, A. Rullan, A. Wilkins, K. Schlegelmilch, I. Roxanis, K.I. Anderson, P.A. Bates, E. Sahai, A FIJI macro for quantifying pattern in extracellular matrix, *Life Sci. Alliance* 4 (3) (2021).
- [19] Z. Puspoki, M. Storath, D. Sage, M. Unser, Transforms and operators for directional bioimage analysis: a survey, *Adv. Anat. Embryol. Cell Biol.* 219 (2016) 69–93.
- [20] S. Wu, H. Li, H. Yang, X. Zhang, Z. Li, S. Xu, Quantitative analysis on collagen morphology in aging skin based on multiphoton microscopy, *J. Biomed. Opt.* 16 (4) (2011) 040502.
- [21] R.M. Williams, W.R. Zipfel, W.W. Webb, Interpreting second-harmonic generation images of collagen I fibrils, *Biophys. J.* 88 (2) (2005) 1377–1386.
- [22] R. Sennett, Z. Wang, A. Rezza, L. Grisanti, N. Roitershtein, C. Sicchio, K.W. Mok, N.J. Heitman, C. Clavel, A. Ma'ayan, M. Rendl, An integrated transcriptome atlas of embryonic hair follicle progenitors, their niche, and the developing skin, *Dev. Cell* 34 (5) (2015) 577–591.
- [23] M.A. Farage, K.W. Miller, P. Elsner, H.I. Maibach, Characteristics of the aging skin, *Adv. Wound Care* 2 (1) (2013) 5–10 (New Rochelle).
- [24] E. Russell-Goldman, G.F. Murphy, The pathobiology of skin aging: new insights into an old dilemma, *Am. J. Pathol.* 190 (7) (2020) 1356–1369.
- [25] M.C. Salzer, A. Lafzi, A. Berenguer-Llargo, C. Youssif, A. Castellanos, G. Solanas, F.O. Peixoto, C. Stephan-Otto Attolini, N. Prats, M. Aguilera, J. Martin-Caballero, H. Heyn, S.A. Benitah, Identity noise and adipogenic traits characterize dermal fibroblast aging, *Cell* 175 (6) (2018) 1575–1590 e22.
- [26] Y. Zhuang, J. Lyga, Inflammaging in skin and other tissues - the roles of complement system and macrophage, *Inflamm. Allergy Drug Targets* 13 (3) (2014) 153–161.
- [27] A. Naba, K.R. Clauser, H. Ding, C.A. Whittaker, S.A. Carr, R.O. Hynes, The extracellular matrix: tools and insights for the "omics" era, *Matrix Biol.* 49 (2016) 10–24.
- [28] H.G. Vogel, Correlation between tensile strength and collagen content in rat skin. Effect of age and cortisol treatment, *Connect Tissue Res.* 2 (3) (1974) 177–182.
- [29] P. Fratzl, *Collagen: Structure and Mechanics*, Springer, New York, 2008.

- [30] M.J. Buehler, Nanomechanics of collagen fibrils under varying cross-link densities: atomistic and continuum studies, *J. Mech. Behav. Biomed. Mater.* 1 (1) (2008) 59–67.
- [31] W. Wilson, C.C. van Donkelaar, J.M. Huyghe, A comparison between mechano-electrochemical and biphasic swelling theories for soft hydrated tissues, *J. Biomech. Eng.* 127 (1) (2005) 158–165.
- [32] W. Ehlers, N. Karajan, B. Markert, An extended biphasic model for charged hydrated tissues with application to the intervertebral disc, *Biomech. Model. Mechanobiol.* 8 (3) (2009) 233–251.
- [33] A.E. Ehret, K. Bircher, A. Stracuzzi, V. Marina, M. Zundel, E. Mazza, Inverse poroelasticity as a fundamental mechanism in biomechanics and mechanobiology, *Nat. Commun.* 8 (1) (2017) 1002.
- [34] E.H. Kobayashi, T. Suzuki, R. Funayama, T. Nagashima, M. Hayashi, H. Sekine, N. Tanaka, T. Moriguchi, H. Motohashi, K. Nakayama, M. Yamamoto, Nrf2 suppresses macrophage inflammatory response by blocking proinflammatory cytokine transcription, *Nat. Commun.* 7 (2016) 11624.
- [35] S. Kurinna, M. Schafer, P. Ostano, E. Karouzakis, G. Chiorino, W. Bloch, A. Bachmann, S. Gay, D. Garrod, K. Lefort, G.P. Dotto, H.D. Beer, S. Werner, A novel Nrf2-miR-29-desmocollin-2 axis regulates desmosome function in keratinocytes, *Nat. Commun.* 5 (2014) 5099.
- [36] C.L. Gallant-Behm, J. Piper, J.M. Lynch, A.G. Seto, S.J. Hong, T.A. Mustoe, C. Maari, L.A. Pestano, C.M. Dalby, A.L. Jackson, P. Rubin, W.S. Marshall, A MicroRNA-29 mimic (Remlarsen) represses extracellular matrix expression and fibroplasia in the skin, *J. Investig. Dermatol.* 139 (5) (2019) 1073–1081.
- [37] P. Pakshir, N. Noskovicova, M. Lodyga, D.O. Son, R. Schuster, A. Goodwin, H. Karvonen, B. Hinz, The myofibroblast at a glance, *J. Cell Sci.* 133 (13) (2020) jcs227900.
- [38] L. Sole-Boldo, G. Raddatz, S. Schutz, J.P. Mallm, K. Rippe, A.S. Lonsdorf, M. Rodriguez-Paredes, F. Lyko, Single-cell transcriptomes of the human skin reveal age-related loss of fibroblast priming, *Commun. Biol.* 3 (1) (2020) 188.
- [39] A. Hirota, Y. Kawachi, K. Itoh, Y. Nakamura, X. Xu, T. Banno, T. Takahashi, M. Yamamoto, F. Otsuka, Ultraviolet A irradiation induces NF-E2-related factor 2 activation in dermal fibroblasts: protective role in UVA-induced apoptosis, *J. Investig. Dermatol.* 124 (4) (2005) 825–832.
- [40] S. Bancelin, B. Lynch, C. Bonod-Bidaud, G. Ducourthial, S. Psilodimitrakopoulos, P. Dokladal, J.M. Allain, M.C. Schanne-Klein, F. Ruggiero, *Ex vivo* multiscale quantitation of skin biomechanics in wild-type and genetically-modified mice using multiphoton microscopy, *Sci. Rep.* 5 (2015) 17635.
- [41] B. Lynch, C. Bonod-Bidaud, G. Ducourthial, J.S. Affagard, S. Bancelin, S. Psilodimitrakopoulos, F. Ruggiero, J.M. Allain, M.C. Schanne-Klein, How aging impacts skin biomechanics: a multiscale study in mice, *Sci. Rep.* 7 (1) (2017) 13750.
- [42] M. Pensalfini, E. Haertel, R. Hopf, M. Wietecha, S. Werner, E. Mazza, The mechanical fingerprint of murine excisional wounds, *Acta Biomater.* 65 (2018) 226–236.
- [43] G. Grieb, G. Steffens, N. Pallua, J. Bernhagen, R. Bucala, Circulating fibrocytes—biology and mechanisms in wound healing and scar formation, *Int. Rev. Cell Mol. Biol.* 291 (2011) 1–19.
- [44] S. Mascharak, H.E. desJardins-Park, M.F. Davitt, M. Griffin, M.R. Borrelli, A.L. Moore, K. Chen, B. Duoto, M. Chinta, D.S. Foster, A.H. Shen, M. Januszyk, S.H. Kwon, G. Wernig, D.C. Wan, H.P. Lorenz, G.C. Gurtner, M.T. Longaker, Preventing engrailed-1 activation in fibroblasts yields wound regeneration without scarring, *Science* 372 (6540) (2021) eaba2374.
- [45] P. Hiebert, The Nrf2 transcription factor: a multifaceted regulator of the extracellular matrix, *Matrix Biol. Plus* 10 (2021) 100057.
- [46] N. Wakabayashi, K. Itoh, J. Wakabayashi, H. Motohashi, S. Noda, S. Takahashi, S. Imakado, T. Kotsuji, F. Otsuka, D.R. Roop, T. Harada, J.D. Engel, M. Yamamoto, Keap1-null mutation leads to postnatal lethality due to constitutive Nrf2 activation, *Nat. Genet.* 35 (3) (2003) 238–245.
- [47] P.M. Elias, Structure and function of the stratum corneum extracellular matrix, *J. Investig. Dermatol.* 132 (9) (2012) 2131–2133.
- [48] G. Latella, Redox imbalance in intestinal fibrosis: beware of the TGFbeta-1, ROS, and Nrf2 connection, *Dig Dis Sci* 63 (2) (2018) 312–320.
- [49] J. Grosche, J. Meissner, J.A. Eble, More than a syllable in fib-ROS-is: the role of ROS on the fibrotic extracellular matrix and on cellular contacts, *Mol. Asp. Med.* 63 (2018) 30–46.
- [50] N. Kaviani, S. Mehlal, M. Jeljeli, N.E.B. Saidu, C. Nicco, O. Cerles, S. Chouzenoux, A. Cauvet, C. Camus, M. Ait-Djoudi, C. Chereau, S. Kerdine-Romer, Y. Allanore, F. Batteux, The Nrf2-antioxidant response element signaling pathway controls fibrosis and autoimmunity in scleroderma, *Front. Immunol.* 9 (2018) 1896.
- [51] J.M. Dyer, R.A. Miller, Chronic skin fragility of aging: current concepts in the pathogenesis, recognition, and management of dermatoporosis, *J. Clin. Aesthet. Dermatol.* 11 (1) (2018) 13–18.
- [52] J. Campisi, The role of cellular senescence in skin aging, *J. Investig. Dermatol. Symp. Proc.* 3 (1) (1998) 1–5.
- [53] C.Y. Ho, O. Dreesen, Faces of cellular senescence in skin aging, *Mech. Ageing Dev.* 198 (2021) 111525.
- [54] J. Campisi, Aging, cellular senescence, and cancer, *Annu. Rev. Physiol.* 75 (2013) 685–705.
- [55] D.A. Lewis, J.B. Travers, D.F. Spandau, A new paradigm for the role of aging in the development of skin cancer, *J. Investig. Dermatol.* 129 (3) (2009) 787–791.
- [56] X. Ding, P. Kakanj, M. Leptin, S.A. Eming, Regulation of the wound healing response during aging, *J. Investig. Dermatol.* 141 (4S) (2021) 1063–1070.
- [57] M.A. Nishiguchi, C.A. Spencer, D.H. Leung, T.H. Leung, Aging suppresses skin-derived circulating SDF1 to promote full-thickness tissue regeneration, *Cell Rep.* 25 (13) (2018) 3898.
- [58] A. Hirota, Y. Kawachi, M. Yamamoto, T. Koga, K. Hamada, F. Otsuka, Acceleration of UVB-induced photoageing in Nrf2 gene-deficient mice, *Exp. Dermatol.* 20 (8) (2011) 664–668.
- [59] P. Hiebert, S. Werner, Regulation of wound healing by the Nrf2 transcription factor—more than cytoprotection, *Int. J. Mol. Sci.* 20 (16) (2019) 3856.
- [60] I.P. Trougakos, Nrf2, stress and aging, *Aging* 11 (15) (2019) 5289–5291 (Albany NY).
- [61] E.N. Tsakiri, S. Gumeni, K.K. Iliaki, D. Benaki, K. Vougas, G.P. Sykiotis, V.G. Gorgoulis, E. Mikros, L. Scorrano, I.P. Trougakos, Hyperactivation of Nrf2 increases stress tolerance at the cost of aging acceleration due to metabolic deregulation, *Aging Cell* 18 (1) (2019) e12845.
- [62] D. Ren, N.F. Villeneuve, T. Jiang, T. Wu, A. Lau, H.A. Toppin, D.D. Zhang, Brusatol enhances the efficacy of chemotherapy by inhibiting the Nrf2-mediated defense mechanism, *Proc. Natl. Acad. Sci. U. S. A.* 108 (4) (2011) 1433–1438.

- [63] L. Florin, H. Alter, H.J. Grone, A. Szabowski, G. Schutz, P. Angel, Cre recombinase-mediated gene targeting of mesenchymal cells, *Genesis* 38 (3) (2004) 139–144.
- [64] T.G. Hamilton, R.A. Klinghoffer, P.D. Corrin, P. Soriano, Evolutionary divergence of platelet-derived growth factor alpha receptor signaling mechanisms, *Mol. Cell. Biol.* 23 (11) (2003) 4013–4025.
- [65] E. Andres-Leon, R. Nunez-Torres, A.M. Rojas, miARma-Seq: a comprehensive tool for miRNA, mRNA and circRNA analysis, *Sci. Rep.* 6 (2016) 25749.
- [66] R. Edgar, M. Domrachev, A.E. Lash, Gene expression omnibus: NCBI gene expression and hybridization array data repository, *Nucleic Acids Res.* 30 (1) (2002) 207–210.
- [67] K. Boehnke, N. Mirancea, A. Pavesio, N.E. Fusenig, P. Boukamp, H.J. Stark, Effects of fibroblasts and microenvironment on epidermal regeneration and tissue function in long-term skin equivalents, *Eur. J. Cell Biol.* 86 (11-12) (2007) 731–746.
- [68] M. Berning, S. Pratzel-Wunder, J.R. Bickenbach, P. Boukamp, Three-dimensional *in vitro* skin and skin cancer models based on human fibroblast-derived matrix, *Tissue Eng. Part C Methods* 21 (9) (2015) 958–970.
- [69] A. Wahlsten, M. Pensalfini, A. Stracuzzi, G. Restivo, R. Hopf, E. Mazza, On the compressibility and poroelasticity of human and murine skin, *Biomech. Model. Mechanobiol.* 18 (4) (2019) 1079–1093.
- [70] M.S. Wietecha, M. Pensalfini, M. Cangkrama, B. Muller, J. Jin, J. Brinckmann, E. Mazza, S. Werner, Activin-mediated alterations of the fibroblast transcriptome and matrisome control the biomechanical properties of skin wounds, *Nat. Commun.* 11 (1) (2020) 2604.
- [71] M.V. Kuleshov, M.R. Jones, A.D. Rouillard, N.F. Fernandez, Q. Duan, Z. Wang, S. Koplev, S.L. Jenkins, K.M. Jagodnik, A. Lachmann, M.G. McDermott, C.D. Monteiro, G.W. Gundersen, A. Ma'ayan, Enrichr: a comprehensive gene set enrichment analysis web server 2016 update, *Nucleic Acids Res.* 44 (W1) (2016) W90–W97.
- [72] F. Supek, M. Bosnjak, N. Skunca, T. Smuc, REVIGO summarizes and visualizes long lists of gene ontology terms, *PLoS One* 6 (7) (2011) e21800.
- [73] J. Wang, S. Vasaikar, Z. Shi, M. Greer, B. Zhang, WebGestalt 2017: a more comprehensive, powerful, flexible and interactive gene set enrichment analysis toolkit, *Nucleic Acids Res.* 45 (W1) (2017) W130–W137.